Progresses in deep material networks and materials design

Zeliang Liu, Ph.D., Research Scientist
Livermore Software Technology Corporation (LSTC)
zlliu@lstc.com

1:30~2:40 PM, July 28, 2019

15th U.S. National Congress on Computational Mechanics
Austin, TX, USA

- **Deep Material Network:** Describing multiscale materials by a multi-layer network structure and mechanistic building blocks

- **Physics-based building block:** Two-layer structure with interpretable fitting parameters

- **Machine Learning:** Offline sampling, training and online extrapolation

- **Applications:** Hyperelastic rubber composite under large deformation, polycrystalline materials with rate-dependent crystal plasticity and CFRPs
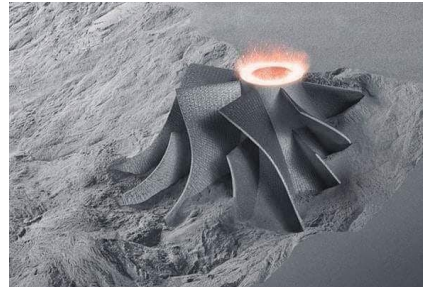
- **Summary and future work**
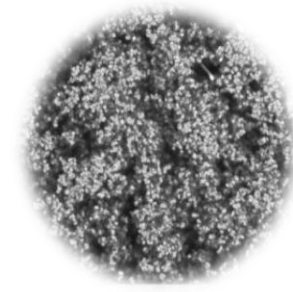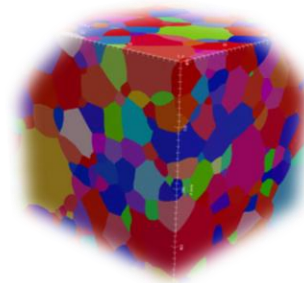
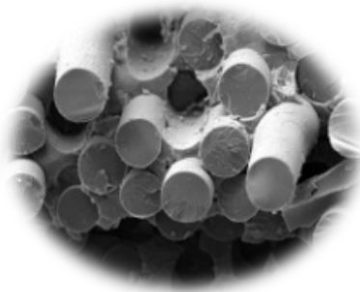**Multiscale nature of modern engineering materials**

Structural analysis

Manufacturing

Materials Design

Representative Volume Element (RVE) and Homogenization

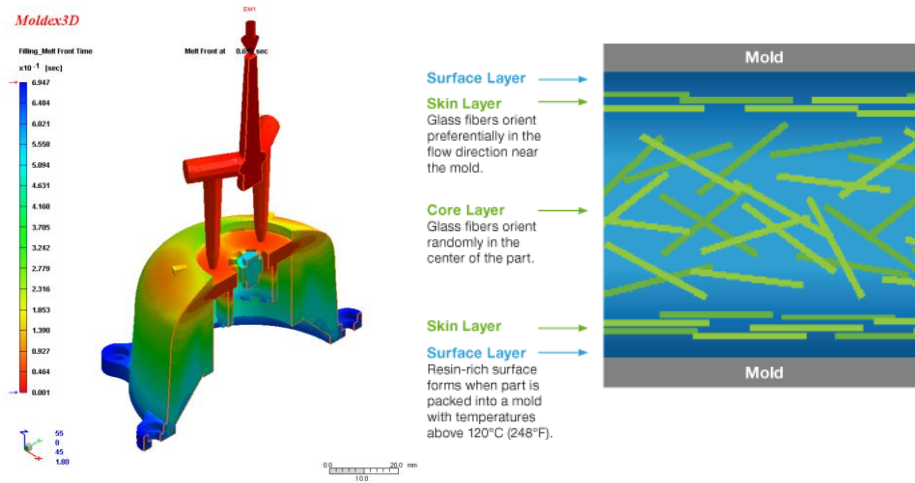Complex Behaviors induced by micro-structures
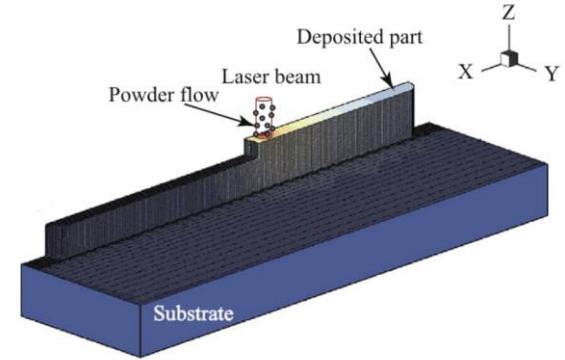
Material evolutions during processing

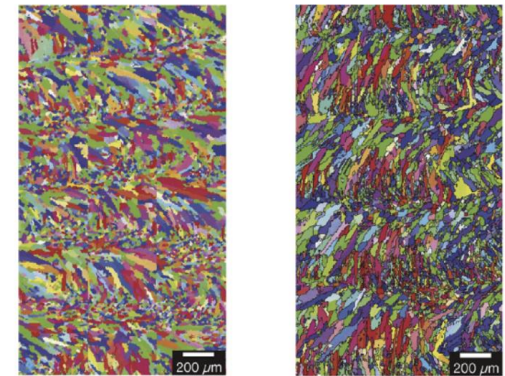Multiscale Physics for design purpose

Injection molding

Additive manufacturing

EBSD images from
uni- and bi-directional scans

Metal forming
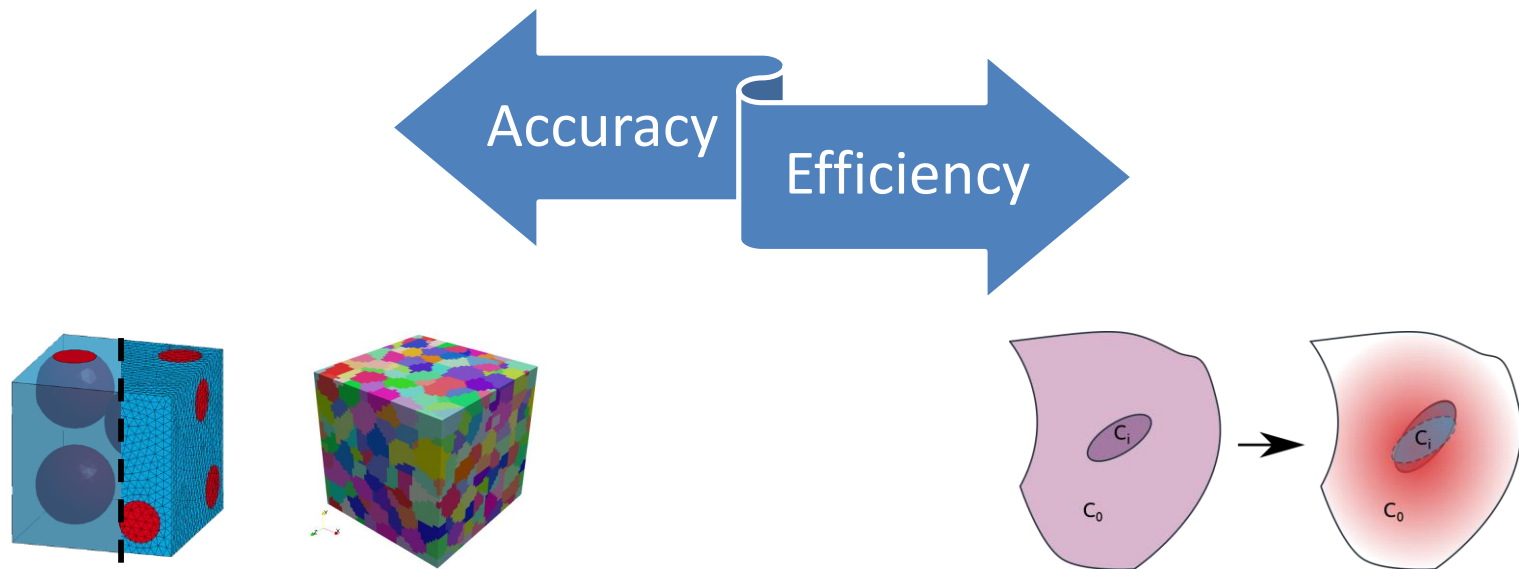
https://materials.imdea.org
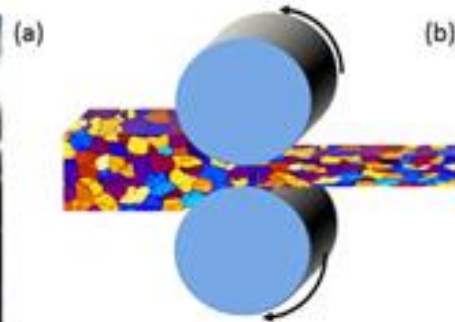
Lian et al., Materials and
Design 2019
Parimi et al., Materials
Characterization 2014

☐ **Objectives:** Arbitrary morphology, material nonlinearity (ex. plasticity, damage), geometric nonlinearities (ex. large deformations).

☐ **Applications:** Concurrent multiscale simulation, materials design …

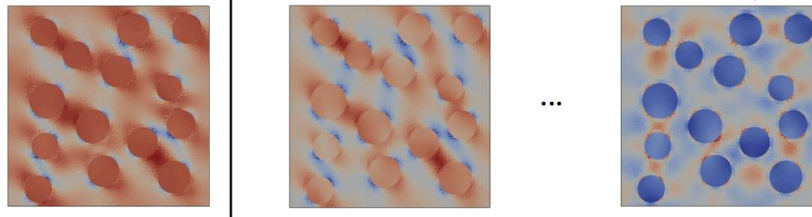**Direct numerical simulation (DNS)**

- Finite element (LSDYNA RVE Package)

- Meshfree and particle methods

- FFT-based method…

Analytical micromechanics methods

- Voigt and Reuss bounds

- Mori-Tanaka method (most popular)
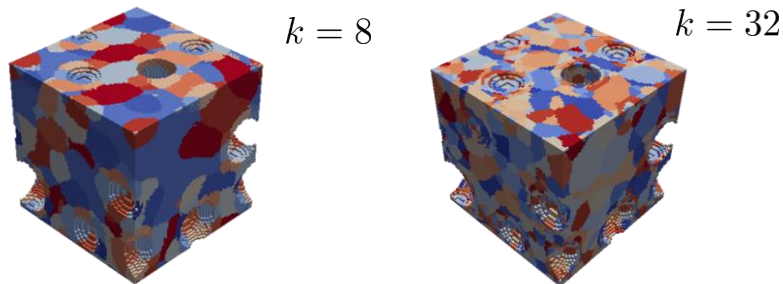
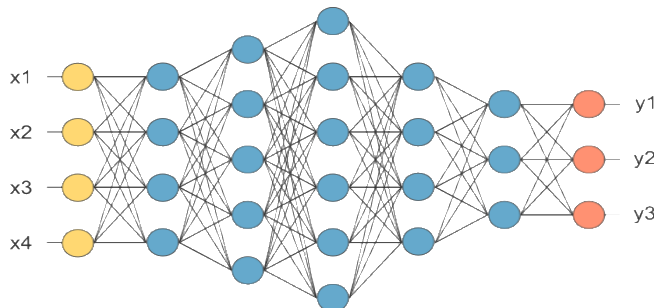- Self-consistent method…

- **Eigen-decomposition:** SVD, PCA, POD ….

Yvonnet and He, JCP 2007;
Oliver et al., CMAME 2018;

- **Clustering analysis:** Self-consistent clustering analysis ….

$k = 8$ $k = 32$

Liu et al., CMAME 2016
Liu et al., CMAME 2018
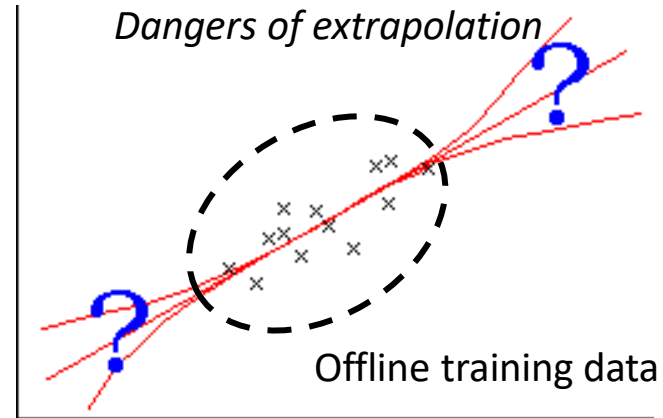*Tang et al., Comput. Mech. 2018*
Yu et al., CMAME 2019

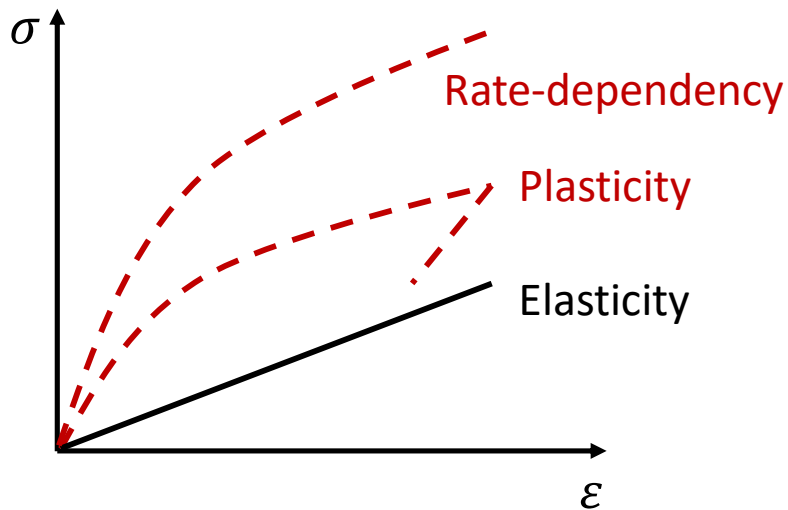- **(Deep) neural network:** CNN, LSTM, Autoencoder …

Ghaboussi et al., JEM 1991
Unger and Konke, Comput. Struct. 2008
Le et al., IJNME 2015
Bessa et al., CMAME 2017
Wand and Sun, CMAME 2018
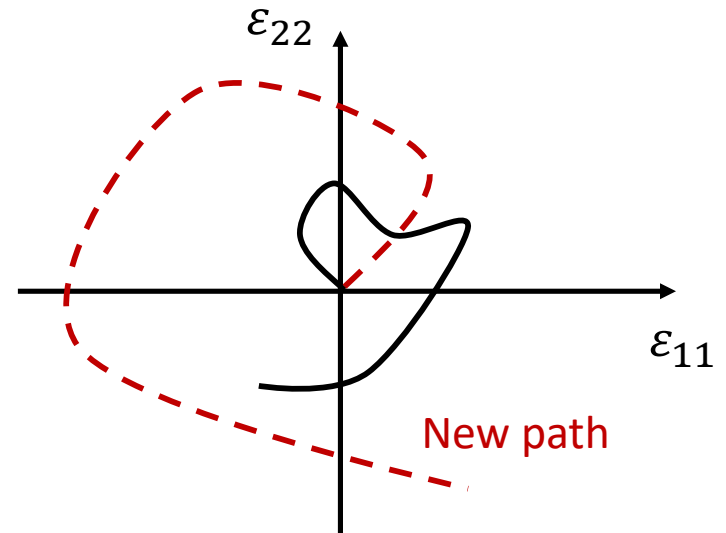*Li et al., Comput. Mech. 2019*
Huang et al. arXiv 2019

The training data is usually limited due to the cost of physical or numerical experiments.
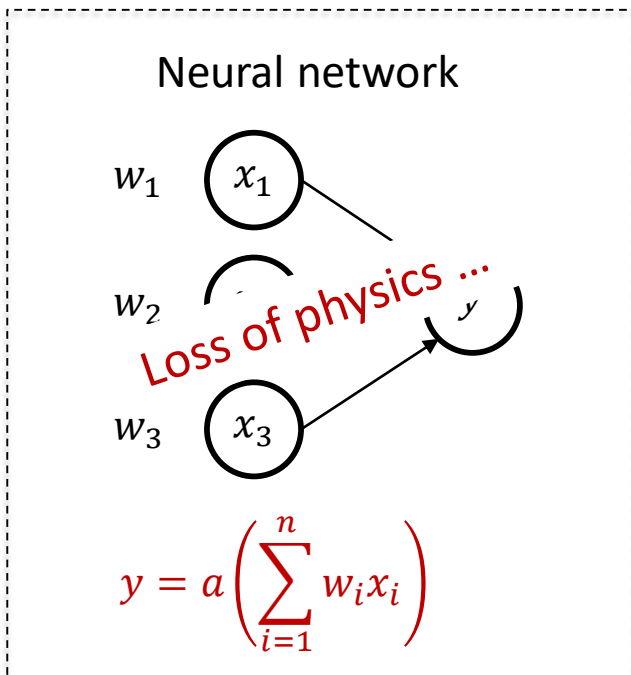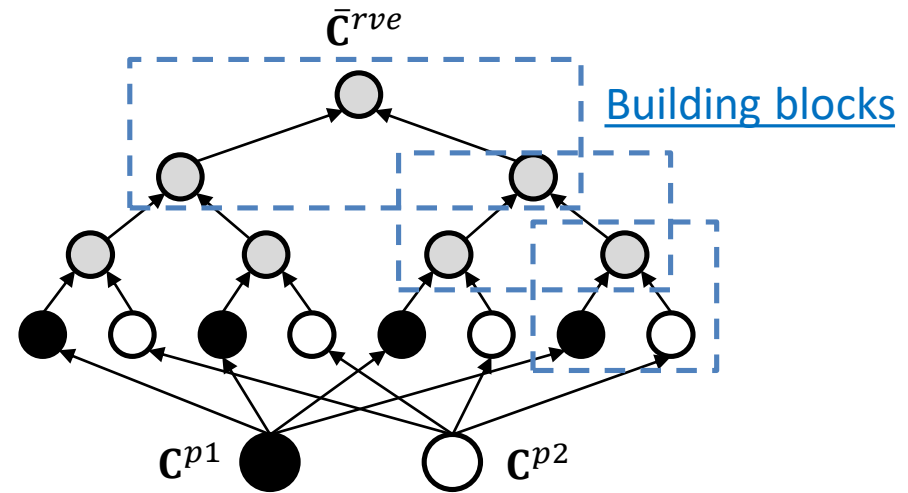
Dangers of extrapolation

Offline training data

1. Unknown material:

Rate-dependency

Plasticity

Elasticity

σ

ε

2. Unknown loading path:

ε_{22}

ε_{11}
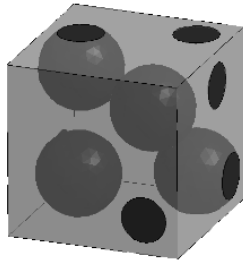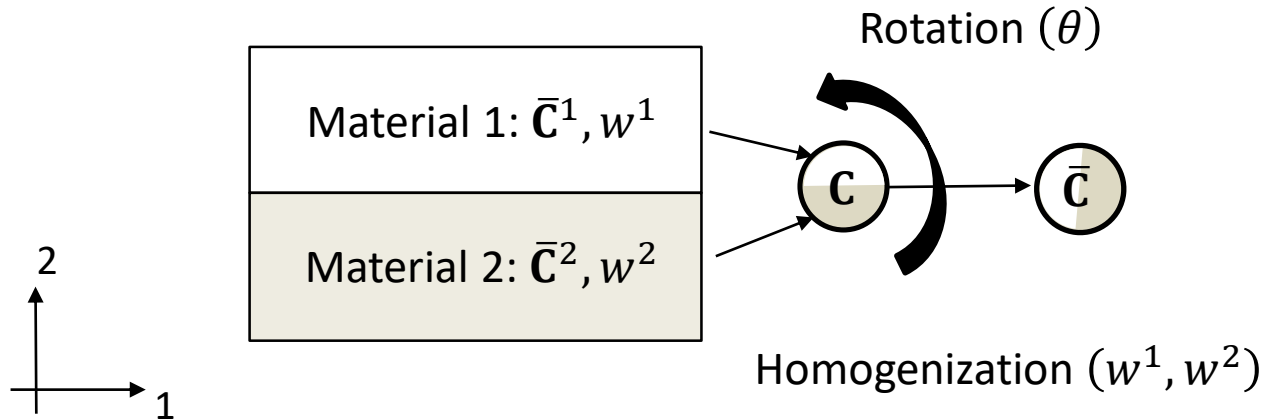
New path

Input: microscale stiffness tensor $\mathbf{C}^{p1}$, $\mathbf{C}^{p2}$

Output: overall stiffness tensor $\bar{\mathbf{C}}^{rve}$

Building blocks

$\bar{\mathbf{C}}^{rve}$

$\mathbf{C}^{p1}$ $\mathbf{C}^{p2}$

Neural network

w_1 x_1

w_2 *Loss of physics ...* y

w_3 x_3

$$y = a\left(\sum_{i=1}^{n} w_i x_i\right)$$

How to embed mechanics/physics into the building block in a network structure?

[1] Z. Liu, C.T. Wu, M. Koishi, CMAME 345 (2019): 1138-1168.
[2] Z. Liu, C.T. Wu, JMPS 127 (2019): 20-46.
[3] Z. Liu, C.T. Wu, M. Koishi, Computational Mechanics (2019)

Rotation (θ)

Material 1: $\bar{\mathbf{C}}^1, w^1$

Material 2: $\bar{\mathbf{C}}^2, w^2$

$\mathbf{C}$ $\bar{\mathbf{C}}$

2

1

Homogenization (w^1, w^2)

- Interfacial equilibrium conditions:

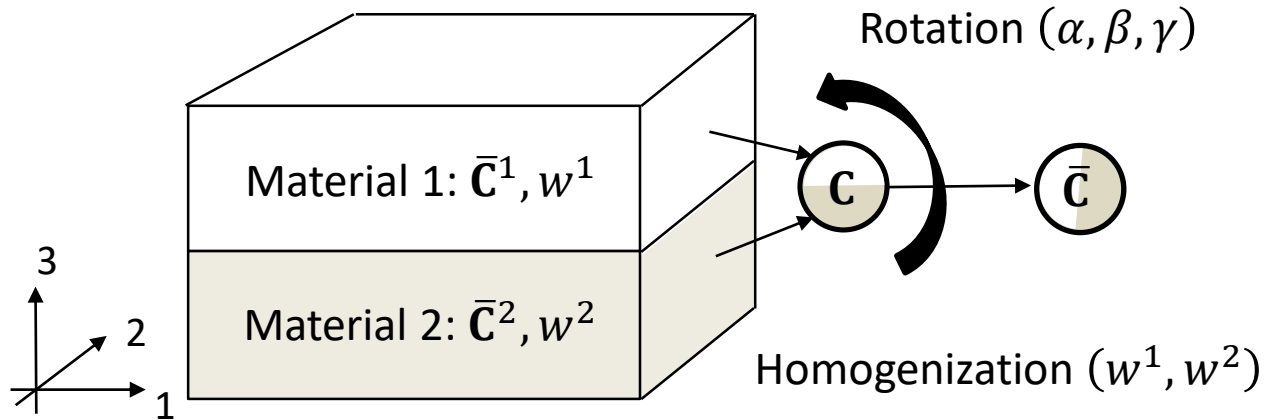$$\sigma_2^1 = \sigma_2^2, \quad \sigma_3^1 = \sigma_3^2$$

- Interfacial kinematic constraints:

$$\varepsilon_1^1 = \varepsilon_1^2$$

- Weights (w^1, w^2) are determined by the activations in the bottom layer

Existence of analytical solutions → **Automatic differentiation**

Rotation (α, β, γ)

Material 1: $\bar{\mathbf{C}}^1, w^1$

Material 2: $\bar{\mathbf{C}}^2, w^2$

Homogenization (w^1, w^2)

- Interfacial equilibrium conditions:

$$\sigma_3^1 = \sigma_3^2, \quad \sigma_4^1 = \sigma_4^2, \quad \sigma_5^1 = \sigma_5^2$$

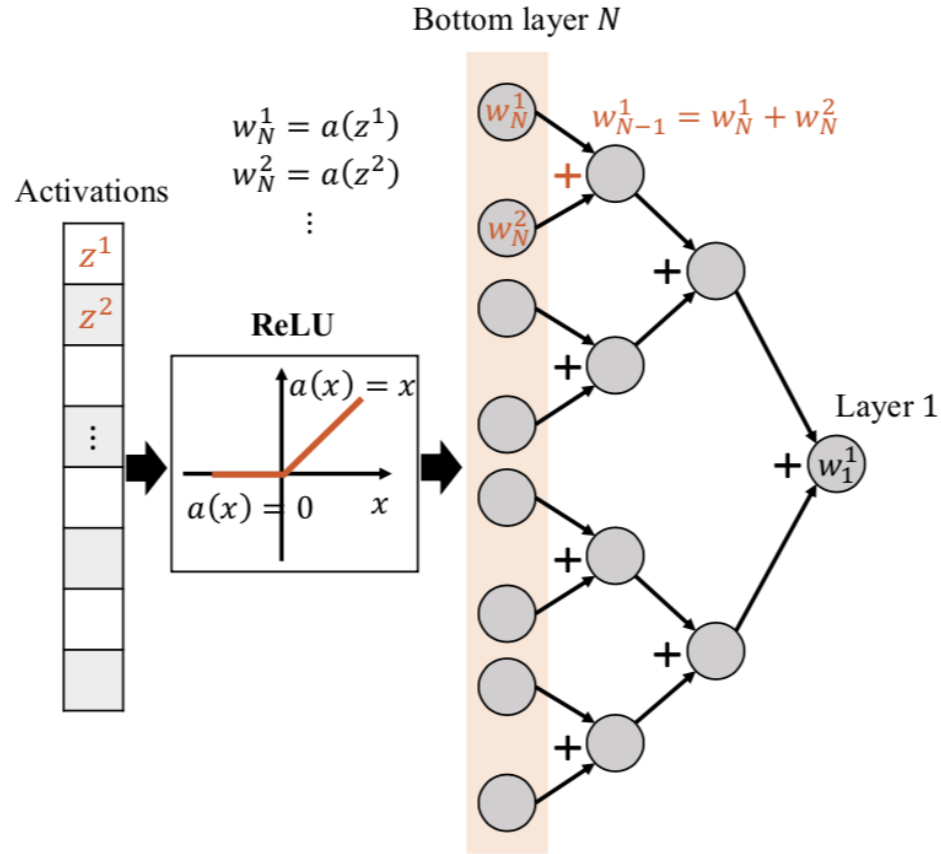- Interfacial kinematic constraints:

$$\varepsilon_1^1 = \varepsilon_1^2, \quad \varepsilon_2^1 = \varepsilon_2^2, \quad \varepsilon_6^1 = \varepsilon_6^2$$

- Weights (w^1, w^2) are determined by the activations in the bottom layer

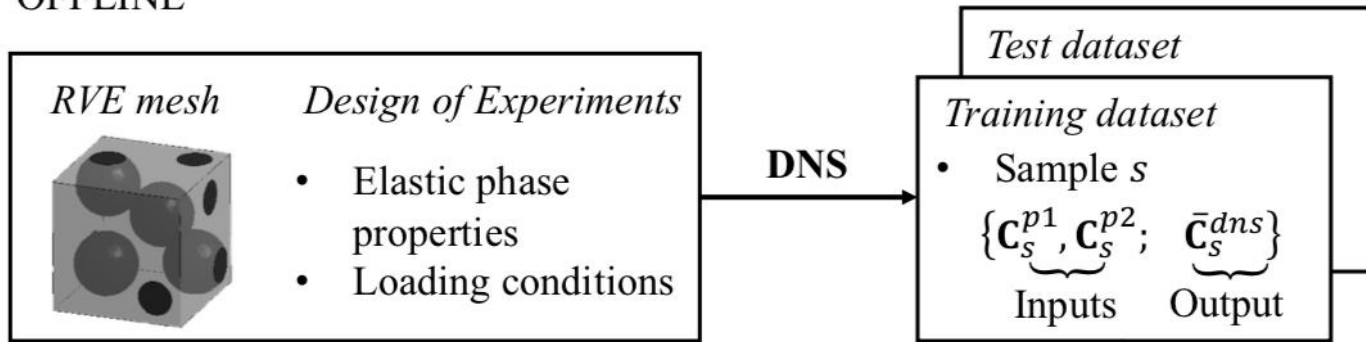**Existence of analytical solutions** ⟶ **Automatic differentiation**

(b) Data flow of weights.

$$\underbrace{\bar{\mathbf{C}}^{rve}}_{\text{Output}} = \mathbf{f}_2(\underbrace{\mathbf{C}^{p1}, \mathbf{C}^{p2}}_{\text{Inputs}}, \overbrace{z^{j=1,2,\dots,2^{N-1}}, \alpha_{i=1,\dots,N}^{k=1,2,\dots,2^{i-1}}, \beta_{i=1,2,\dots,N}^{k=1,2,\dots,2^{i-1}}, \gamma_{i=1,2,\dots,N}^{k=1,2,\dots,2^{i-1}}}^{\text{Fitting parameters}}).$$

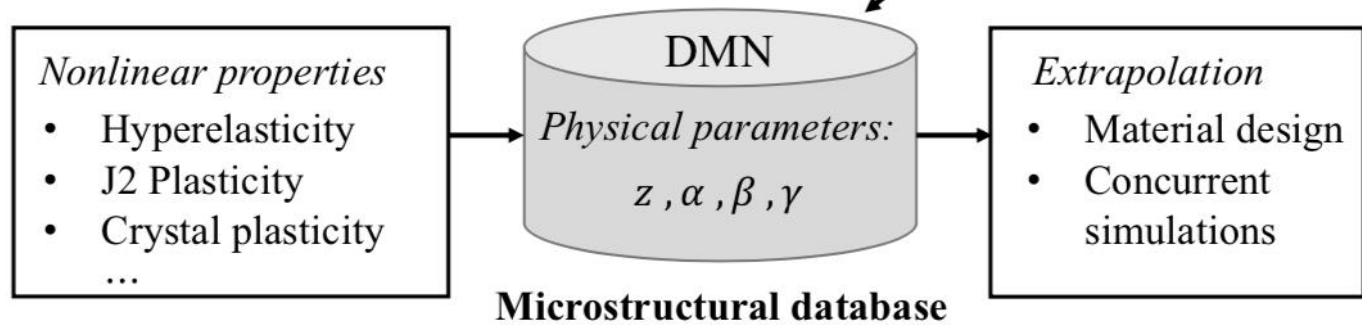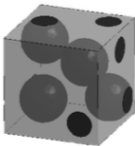Figure 1: Global framework of deep material network illustrated for a 3D two-phase RVE. The stiffness matrices of the two microscale phases are $\mathbf{C}_s^{p1}$ and $\mathbf{C}_s^{p2}$, and $\bar{\mathbf{C}}_s^{dns}$ is the overall stiffness matrices generated by DNS of RVE homogenization. Fitting parameters of DMN include activation z and rotation angles (α, β, γ).

LSTC
Livermore Software
Technology Corp.

OFFLINE

RVE mesh   *Design of Experiments*
- Elastic phase properties
- Loading conditions

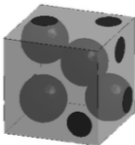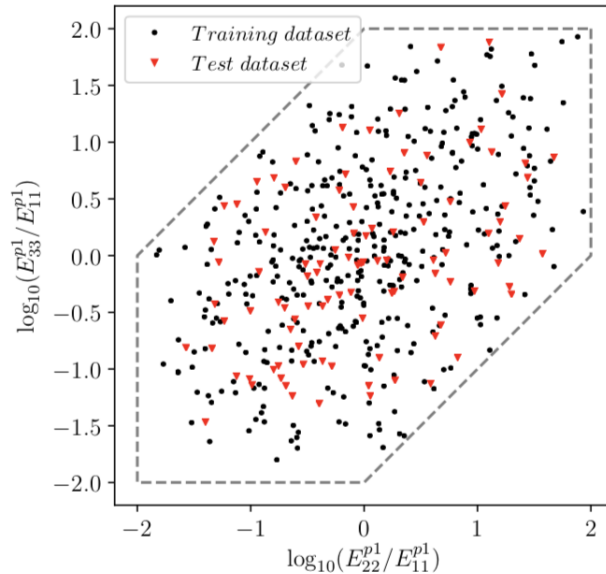## Design of Experiments (DoE)

- Strong material anisotropy and phase contrast
- Analyzed using LS-DYNA RVE package

Sample the compliance matrices of material 1 and 2:

$$\mathbf{D}^{pi} = \begin{Bmatrix} 1/E_{11}^{pi} & -\nu_{12}^{pi}/E_{22}^{pi} & -\nu_{31}^{pi}/E_{11}^{pi} \\ & 1/E_{22}^{pi} & -\nu_{23}^{pi}/E_{33}^{pi} \\ & & 1/E_{33}^{pi} \\ & & & 1/(2G_{23}^{pi}) \\ & & & & 1/(2G_{31}^{pi}) \\ & & & & & 1/(2G_{12}^{pi}) \end{Bmatrix} \quad \text{with } i = 1, 2.$$

LSTC
Livermore Software
Technology Corp.

OFFLINE

RVE mesh	Design of Experiments
	• Elastic phase properties
	• Loading conditions

Design of Experiments (DoE)

- Strong material anisotropy and phase contrast

- Analyzed using LS-DYNA RVE package

(a) Anisotropy of phase 1.
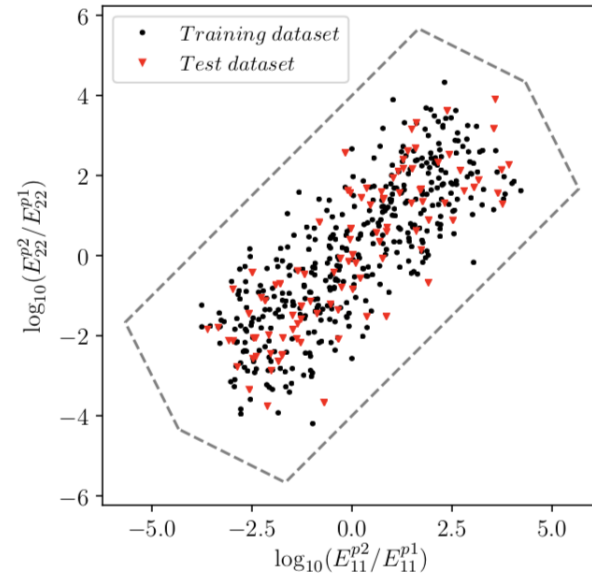
(b) Contrasts of moduli between phase 1 and 2.

Figure 4: Distributions of tension moduli in the training and test datasets for the particle-reinforced RVE. Plots for other material systems are similar, and there are 400 training samples (•) and 100 test samples (▼). The theoretical bounds are shown as the dashed lines.

Cost function for training

$$J(z, \alpha, \beta, \gamma) = \frac{1}{2N_s} \sum_s J_s(z, \alpha, \beta, \gamma) + \lambda \left(\sum_j a(z^j) - 2^{N-2} \right)^2$$
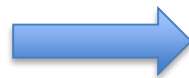
Regularization term

with

$$J_s(z, \alpha, \beta, \gamma) = \frac{||\bar{\mathbf{C}}_s^{dns} - \mathbf{f}_2(\mathbf{C}_s^{p1}, \mathbf{C}_s^{p2}, z, \alpha, \beta, \gamma)||^2}{||\bar{\mathbf{C}}_s^{dns}||^2} \quad \text{for a two-phase RVE,}$$
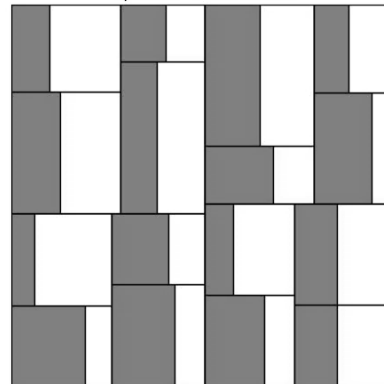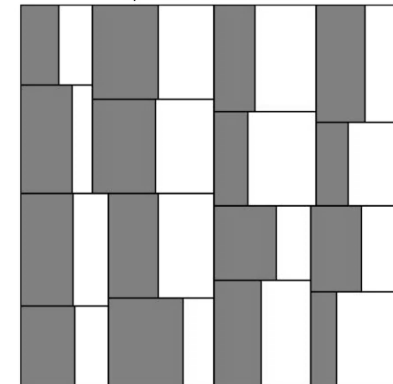
Backpropagation

Stochastic Gradient Descent (SGD)

Automatic network compression

Epoch =   0, vf1 = 0.50

Epoch =   0, vf1 = 0.52
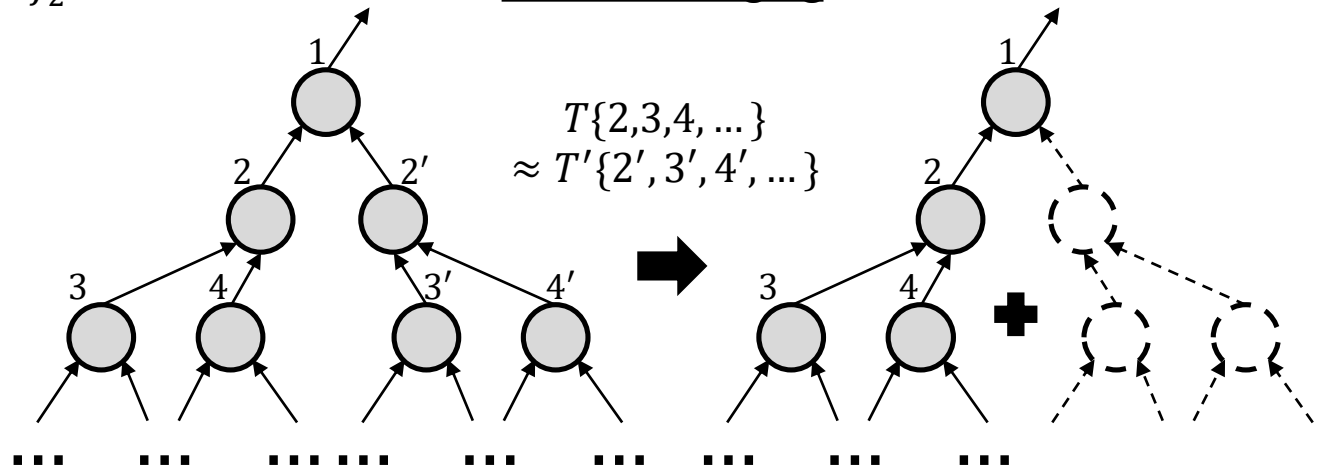
Deletion of node

$f_{(2)} = 1$

- ❑ Network is reordered before the compression.

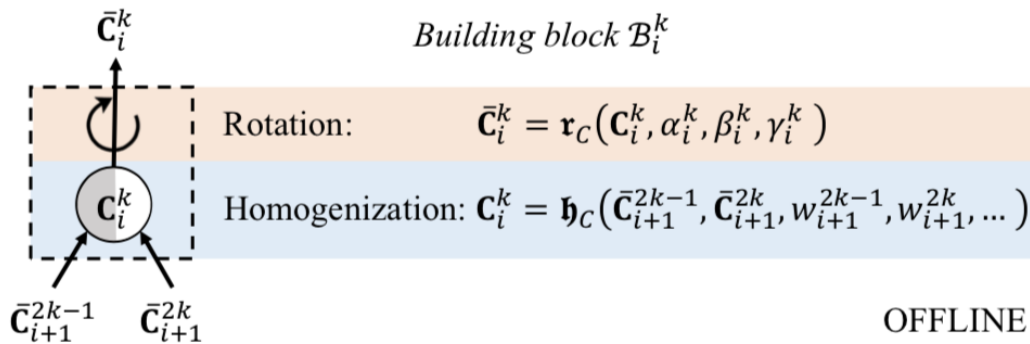- ❑ Network compression operations are performed every 10 epochs.
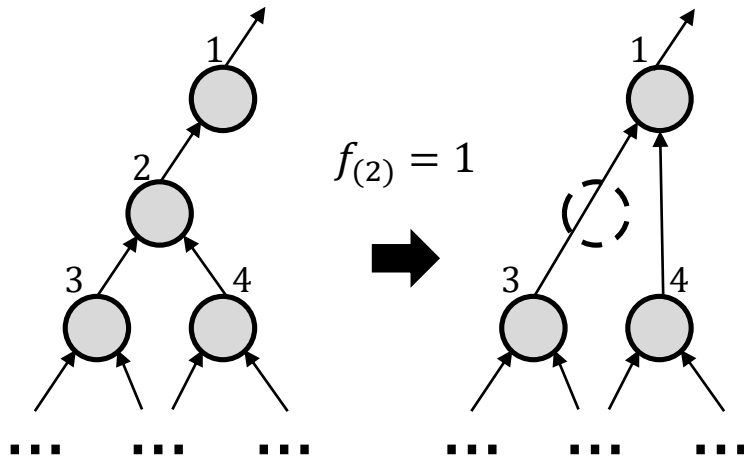
➤ Delete node 2, if $f_2 = 1$

Subtree merging

$T\{2,3,4,\dots\}$
$\approx T'\{2', 3', 4', \dots\}$

➤ Merge subtrees $T\{2,3,4,\dots\}$ and $T'\{2', 3', 4', \dots\}$

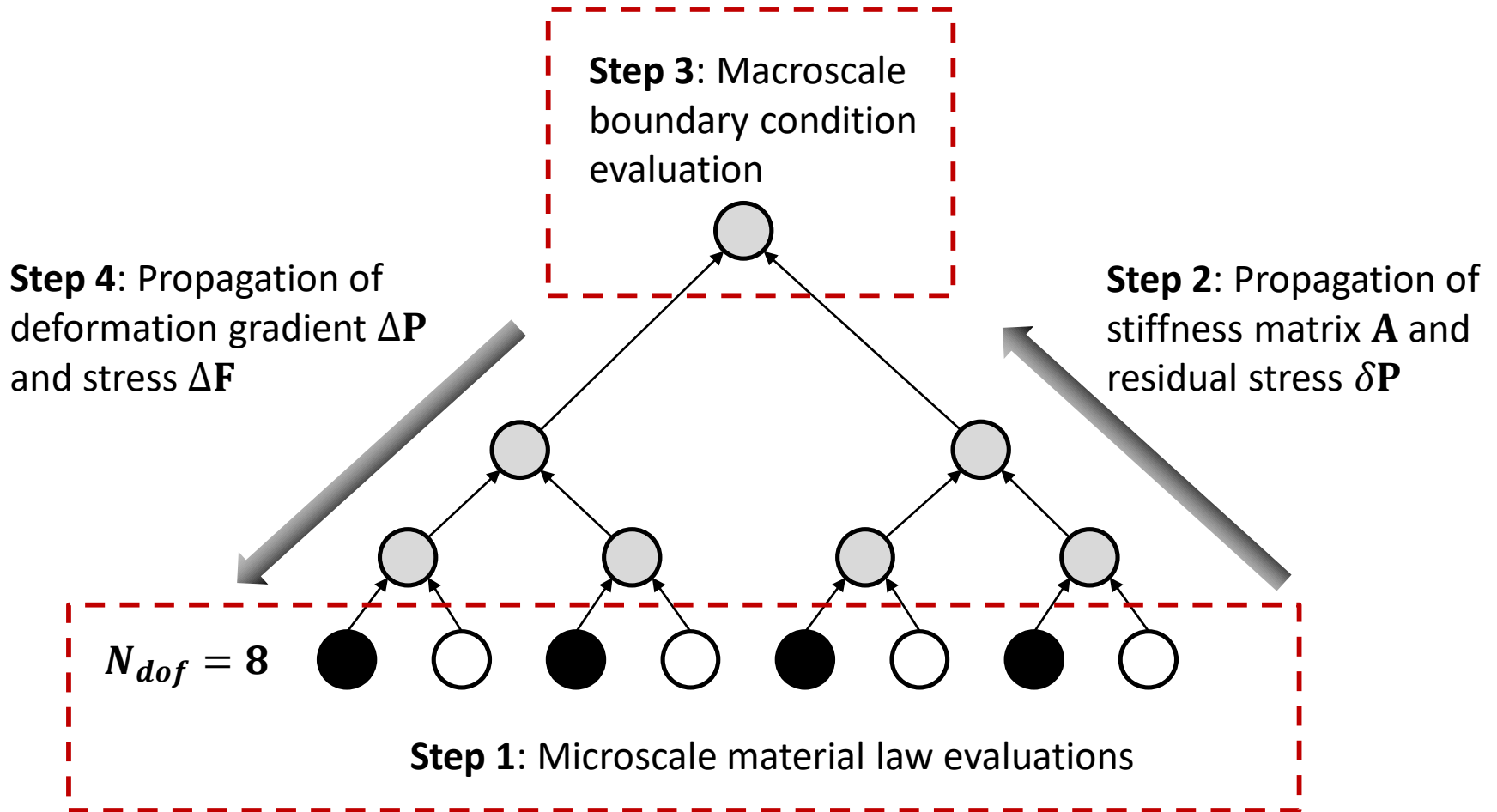**Offline stage:** $\Delta\sigma = \mathbf{C}:\Delta\varepsilon$

Linear elasticity:
No iteration needed

Building block $\mathcal{B}_i^k$

Rotation: $\bar{\mathbf{C}}_i^k = \mathfrak{r}_C(\mathbf{C}_i^k, \alpha_i^k, \beta_i^k, \gamma_i^k)$

Homogenization: $\mathbf{C}_i^k = \mathfrak{h}_C(\bar{\mathbf{C}}_{i+1}^{2k-1}, \bar{\mathbf{C}}_{i+1}^{2k}, w_{i+1}^{2k-1}, w_{i+1}^{2k}, \dots)$

OFFLINE

Online stage: $\Delta\mathbf{P} = \mathbf{A}:\Delta\mathbf{F} + \delta\mathbf{P}$
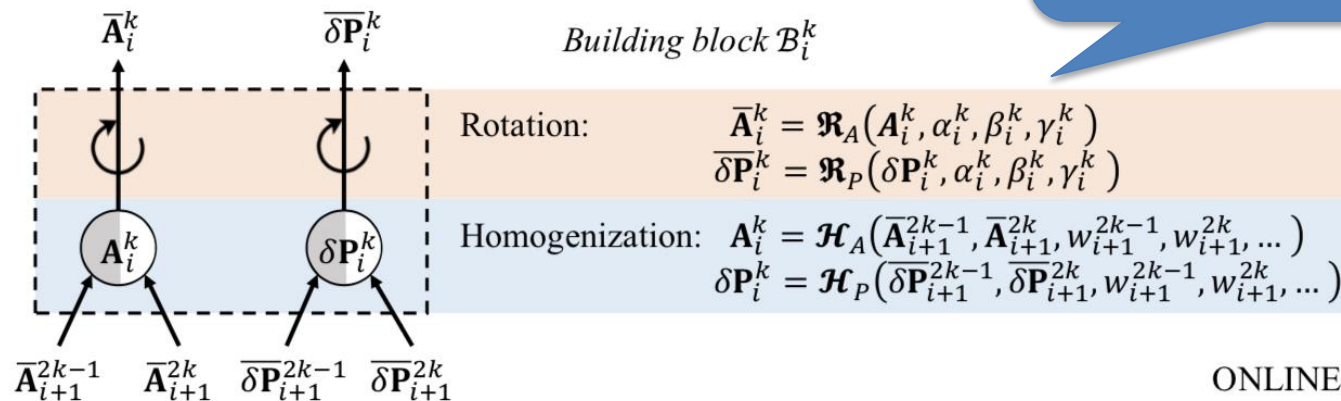
Material and geometric Nonlinearity:
Newton's iterations

Building block $\mathcal{B}_i^k$

Rotation:
$\bar{\mathbf{A}}_i^k = \mathfrak{R}_A(\mathbf{A}_i^k, \alpha_i^k, \beta_i^k, \gamma_i^k)$
$\overline{\delta\mathbf{P}_i^k} = \mathfrak{R}_P(\delta\mathbf{P}_i^k, \alpha_i^k, \beta_i^k, \gamma_i^k)$

Homogenization:
$\mathbf{A}_i^k = \mathcal{H}_A(\bar{\mathbf{A}}_{i+1}^{2k-1}, \bar{\mathbf{A}}_{i+1}^{2k}, w_{i+1}^{2k-1}, w_{i+1}^{2k}, \dots)$
$\delta\mathbf{P}_i^k = \mathcal{H}_P(\overline{\delta\mathbf{P}}_{i+1}^{2k-1}, \overline{\delta\mathbf{P}}_{i+1}^{2k}, w_{i+1}^{2k-1}, w_{i+1}^{2k}, \dots)$

ONLINE

Step 3: Macroscale boundary condition evaluation

Step 4: Propagation of deformation gradient $\Delta \mathbf{P}$ and stress $\Delta \mathbf{F}$

Step 2: Propagation of stiffness matrix $\mathbf{A}$ and residual stress $\delta \mathbf{P}$

$N_{dof} = 8$

Step 1: Microscale material law evaluations

"Computational cost" = $O(N_{dof})$

2D materials:
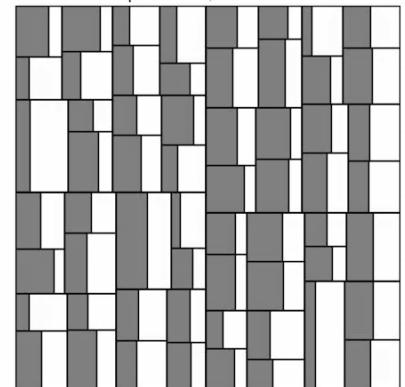
- Mooney-Rivlin hyperelasticity
- Von Mises plasticity

$vf_1 = 0.29, N_{ele} = 3186$ $vf_1 = 0.50, N_{ele} = 9868$ $vf_1 = 0.64, N_{ele} = 4355$

(b) Matrix-inclusion   (c) Amorphous   (d) Anisotropic
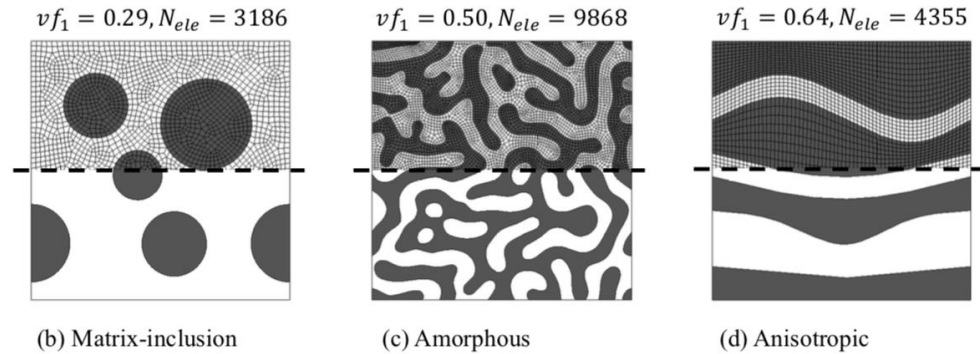
[1] Z. Liu, C.T. Wu, M. Koishi. CMAME 345 (2019): 1138-1168.

3D materials:

- **Mooney-Rivlin hyperelasticity with Mullins effect**
- Von Mises plasticity
- Rate-dependent crystal plasticity

[2] Z. Liu, C.T. Wu. JMPS 127 (2019): 20-46.
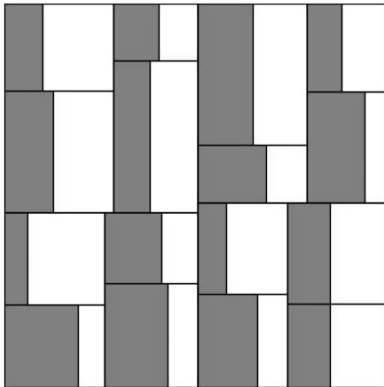
$vf_1 = 22.6\%$

UD composite (Microscale) $vf_1 = 29.4\%$

Woven composite (Mesoscale) $vf_1 = 41.4\%$

LSTC
Livermore Software
Technology Corp.

$N = 5$

$N = 7$

Treemaps: nested rectangles for displaying hierarchical structure

Videos

LSTC
Livermore Software
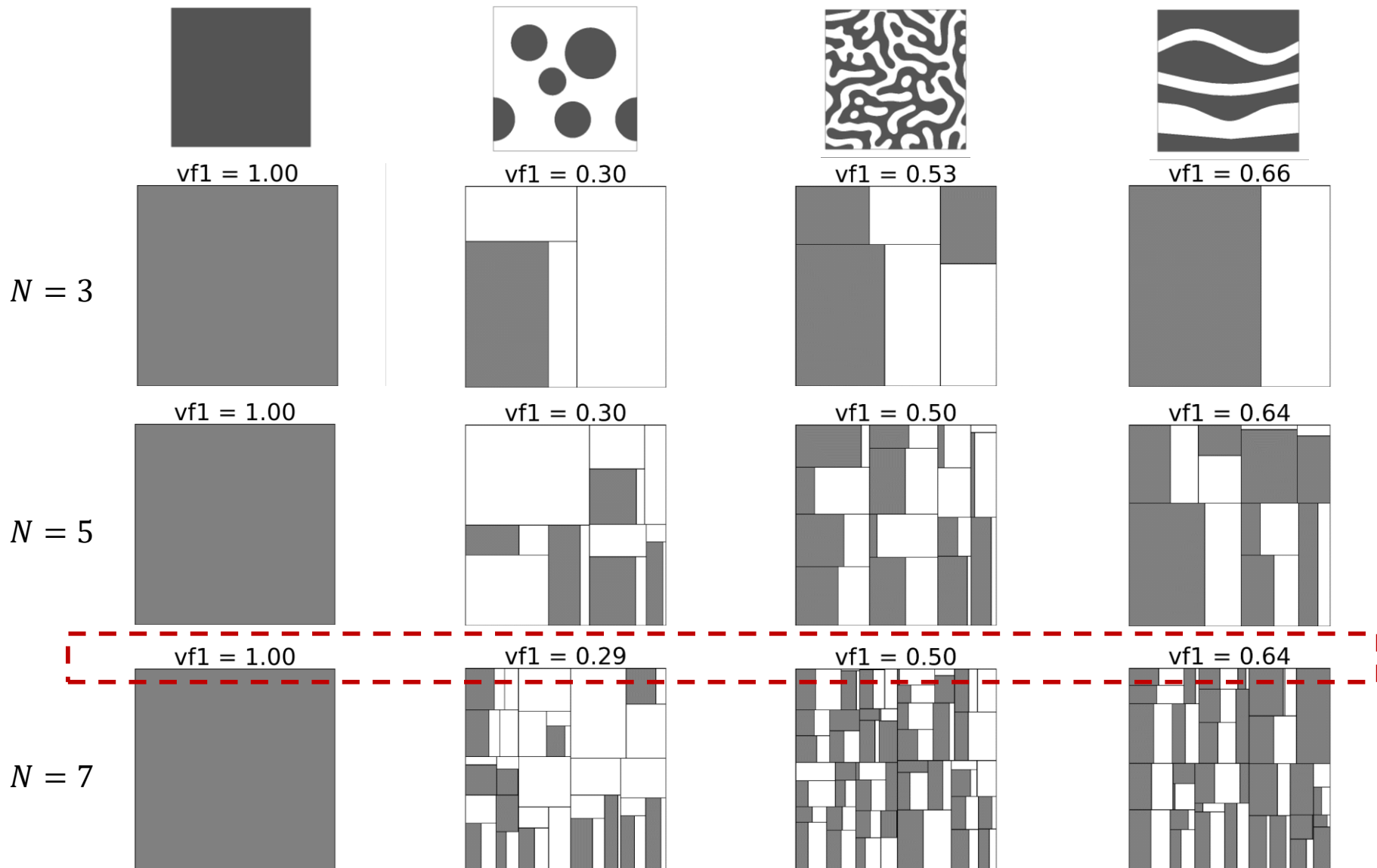Technology Corp.

Training dataset (200): —— Validation dataset (100): – –
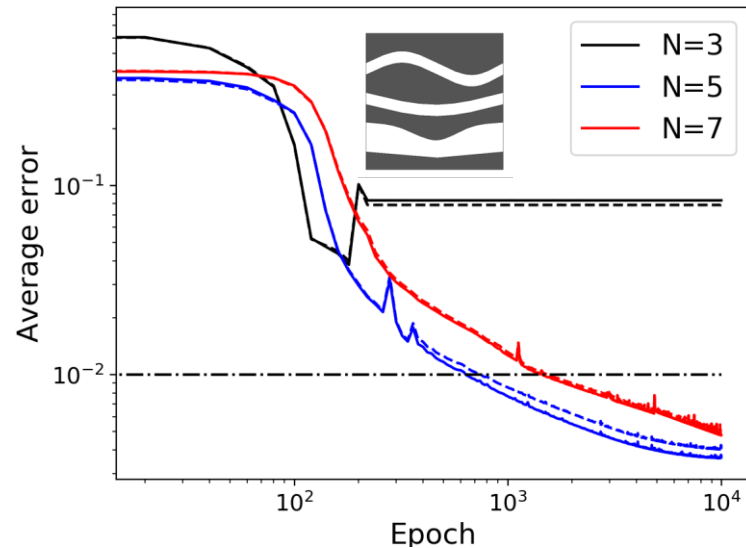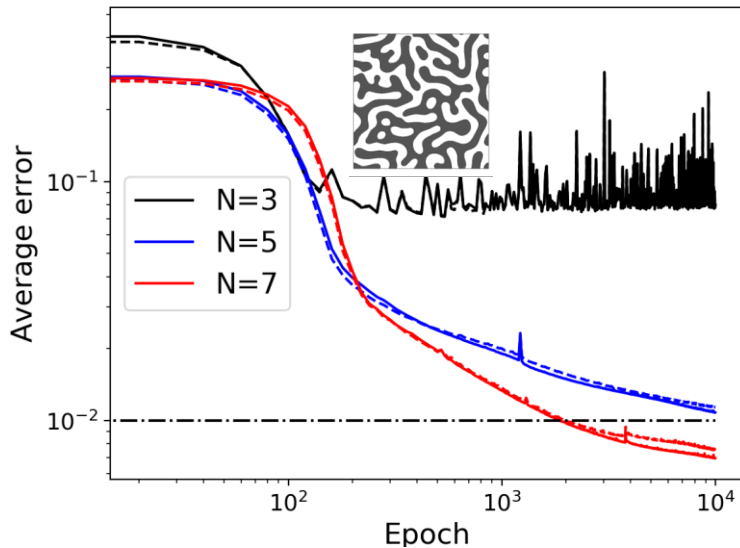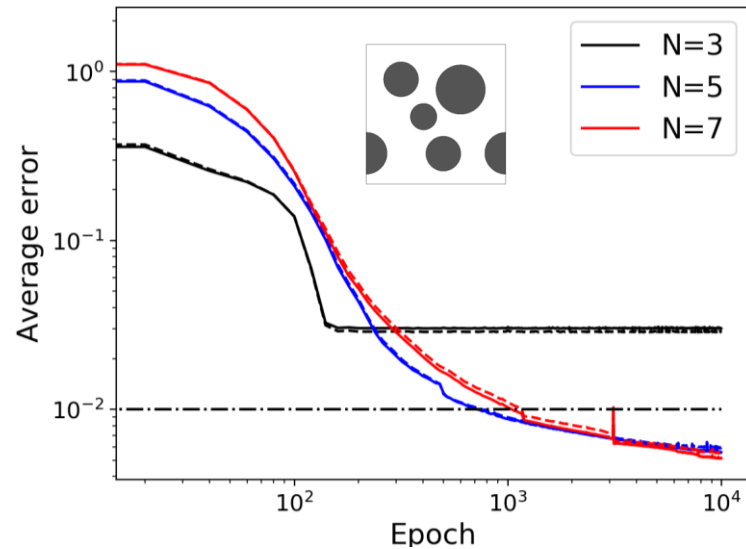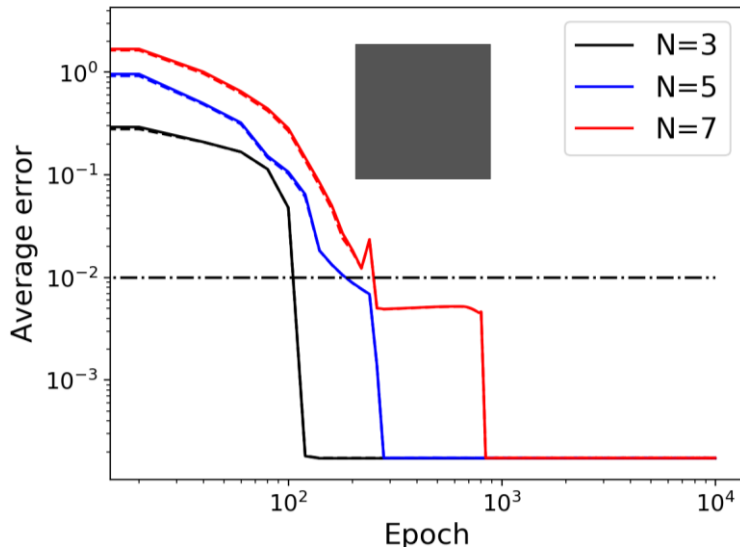
- The maximum stiffness contrast between material phases can go up to 10^4.
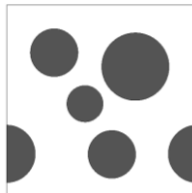- No overfitting is observed (low validation error).
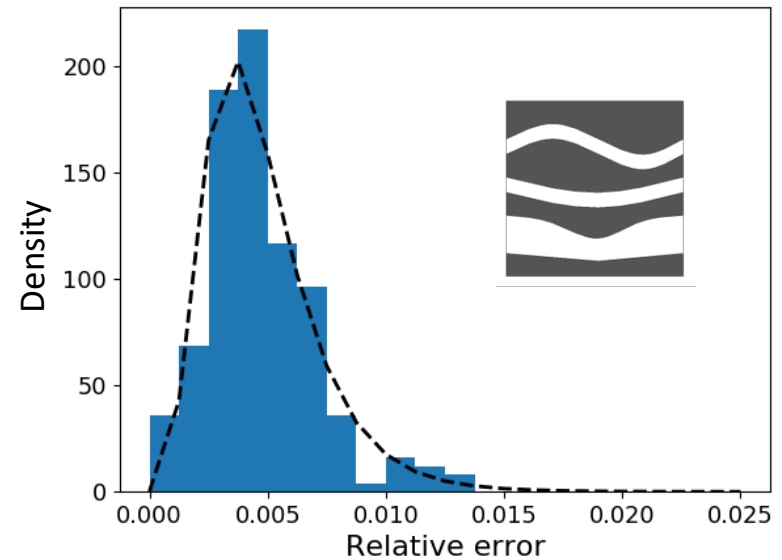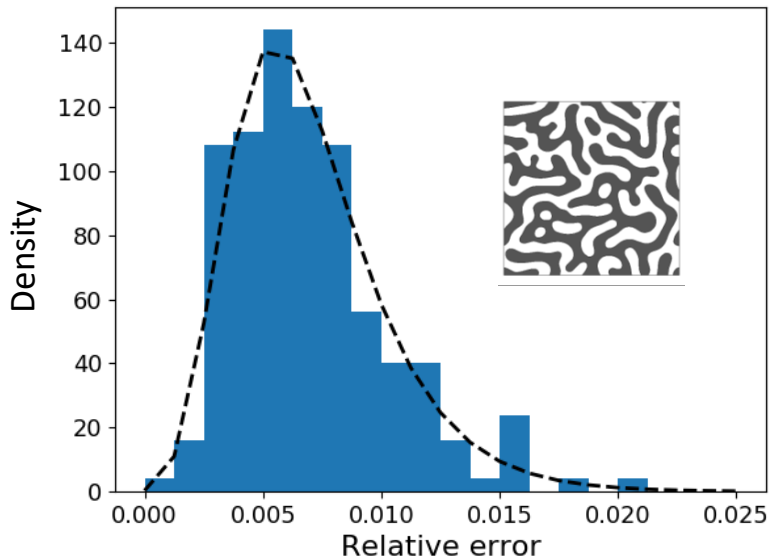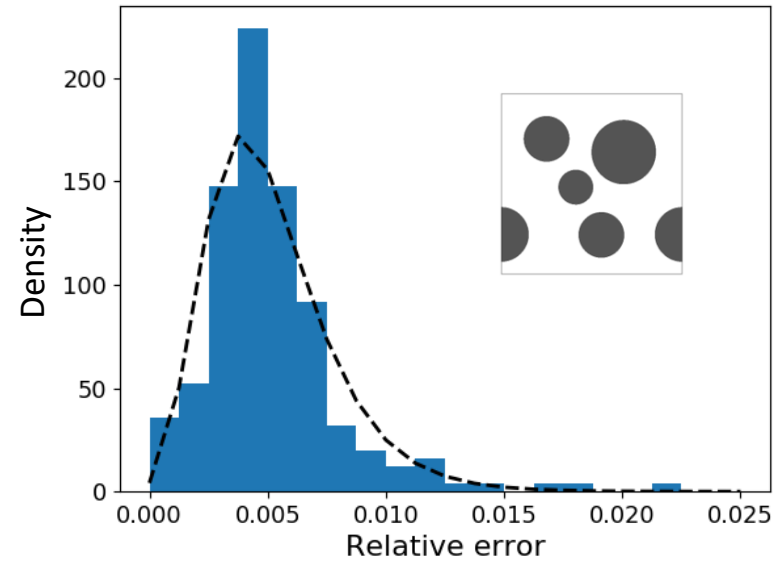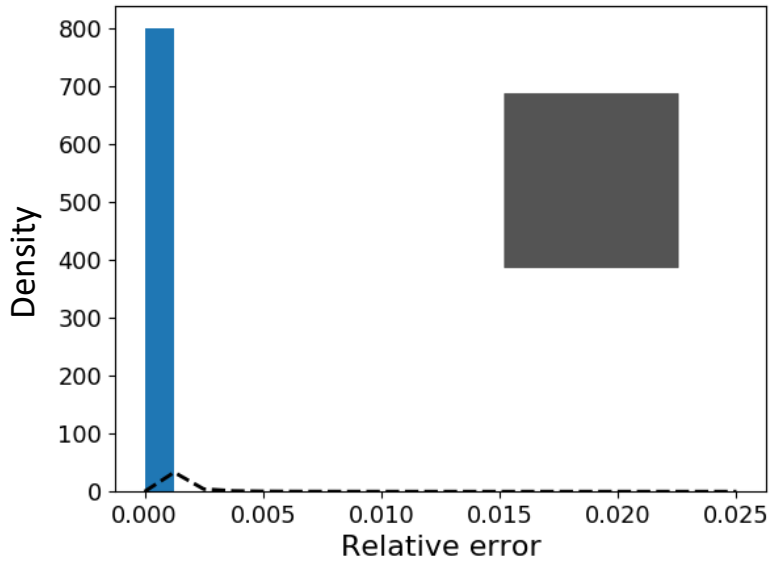
- For each RVE, the maximum error within the 200 samples is below 2.5%.
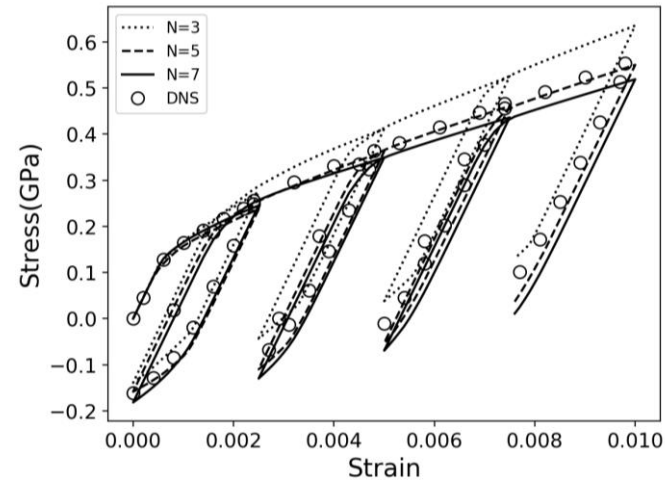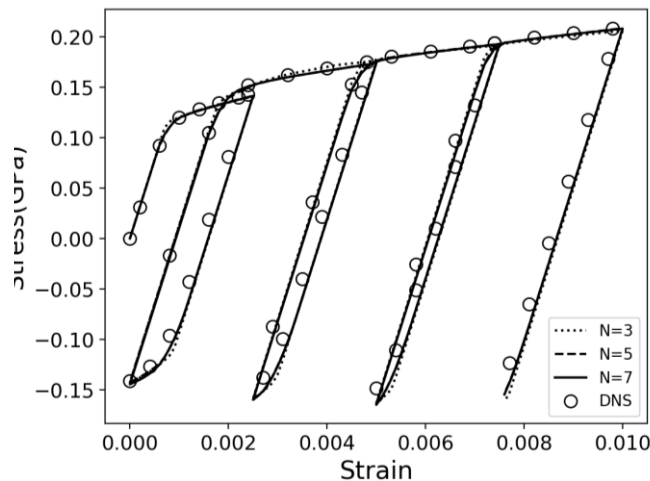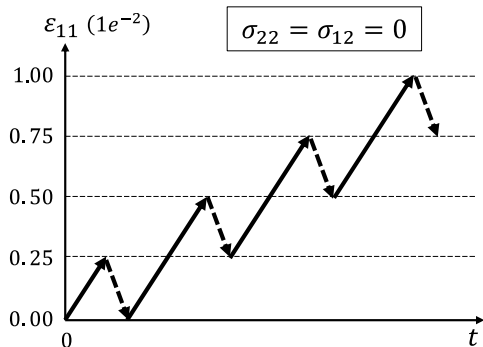
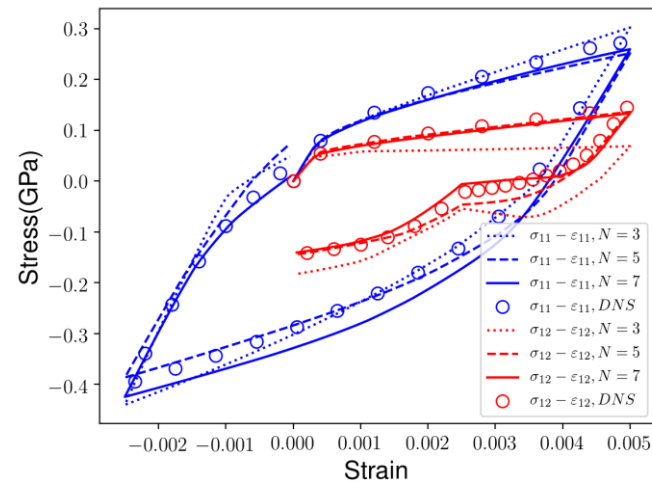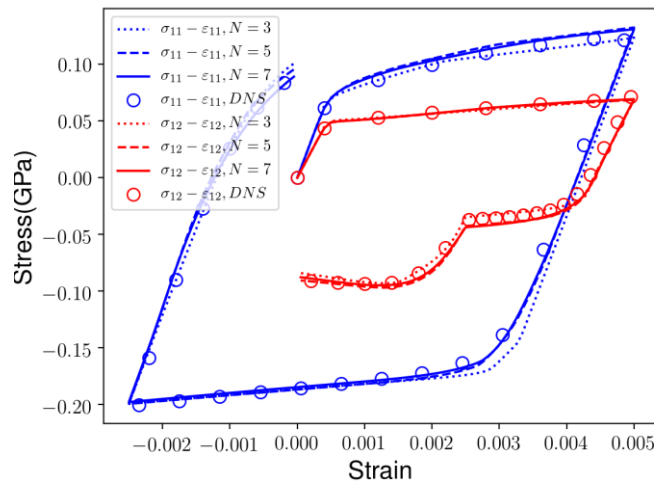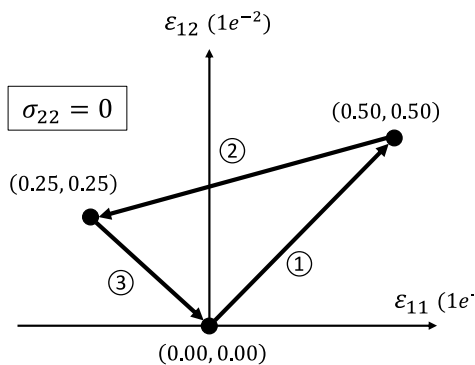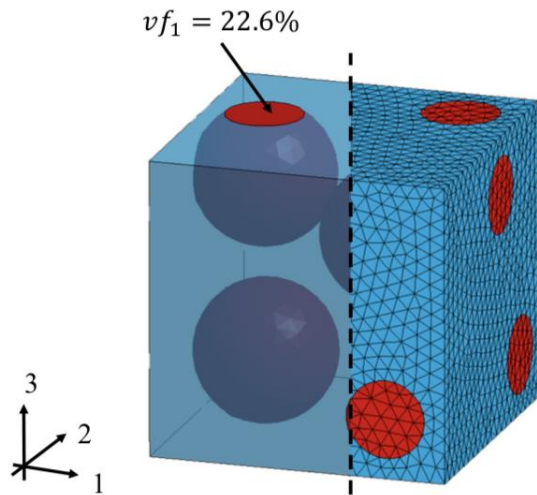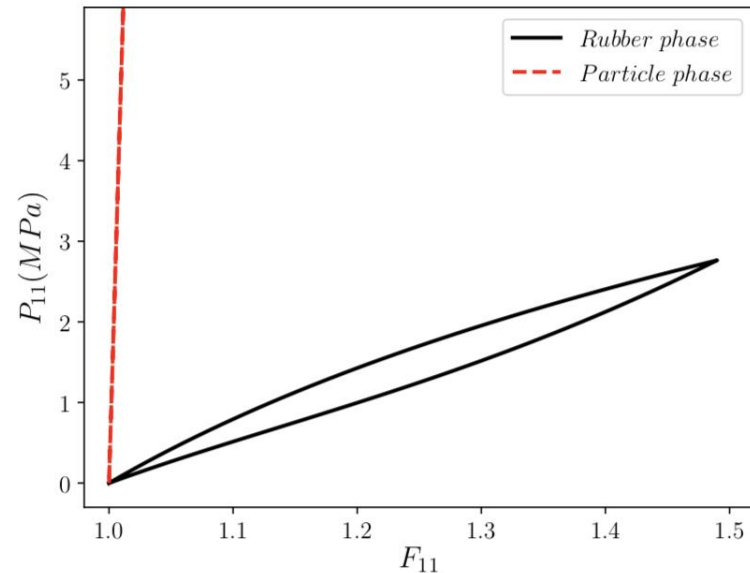Geometric info is learned accurately from mechanical property data

DNS FE model: 84693 nodes and 59628 10-node tetrahedron


(a) Geometry and mesh.

(b) Uniaxial responses of individual phases (online).

Figure 7: Particle reinforced RVE: (a) The volume fraction of the particle phase is 22.6% and the FE model has 84693 nodes and 59628 10-node tetrahedron elements; (b) In the online extrapolation stage, the matrix phase is considered as a Mooney-Rivlin hyperelastic rubber with Mullins effect and the particle is a Neo-Hookean material which is 100 times harder than the matrix.
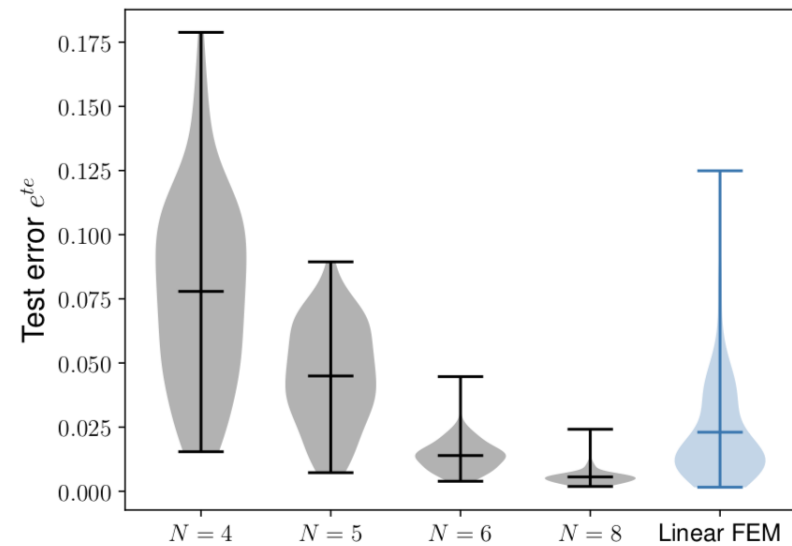
LSTC
Livermore Software
Technology Corp.

DNS FE model: 84693 nodes and 59628 10-node tetrahedron

Linear FE model: 11236 nodes and 59628 4-node tetrahedron
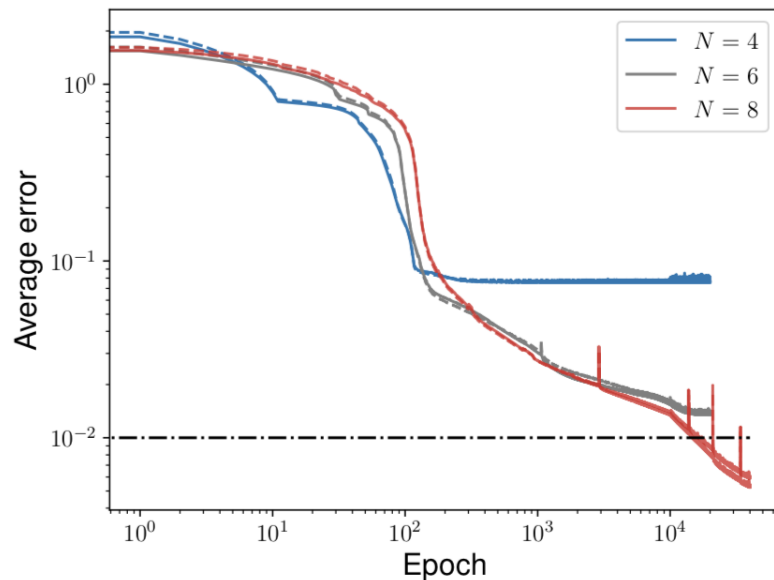
(a) Training histories.

(b) Distributions of test error e^{te}.

Figure 8: Error histories and distribution of DMN for the particle reinforced composite. In (a), the histories of the average training and test errors are denoted by solid and dashed lines, respectively. In (b), the distributions of test error are shown for trained DMNs with various depths (black), and the test result of the linear FE model (blue) is also provided for comparison.

LSTC Livermore Software Technology Corp.

Table 1: Training results of the particle-reinforced composite. Average training error $\bar{e}^{tr}$, average test error $\bar{e}^{tr}$, maximum test error and predicted volume fraction vf_1 are provided for each DMN. Test errors of the linear FEM model are also shown.

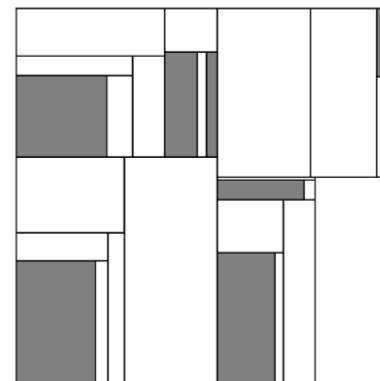|	Epochs	Training $\bar{e}^{tr}$	Test $\bar{e}^{te}$	Maximum e_s^{te}	vf_1
$N = 4$	20000	7.61%	7.79%	17.9%	0.211 (-6.63%)
$N = 5$	20000	4.47%	4.49%	8.94%	0.220 (-2.65%)
$N = 6$	20000	1.34%	1.39%	4.46%	0.220 (-2.65%)
$N = 8$	40000	0.53%	0.59%	2.41%	0.224 (-0.88%)
Linear FEM	\	\	2.30%	12.5%	\

Treemap plot of DMN: Visualization of the binary-tree structure
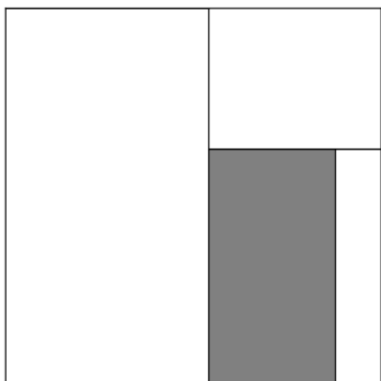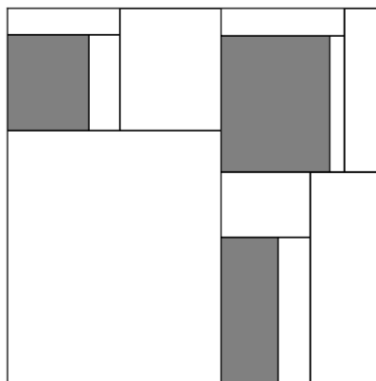
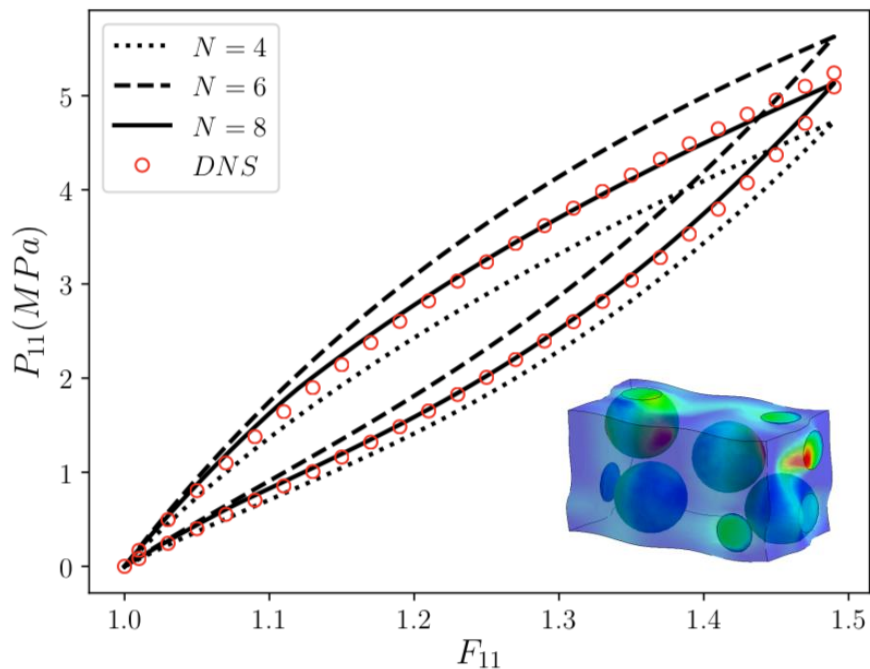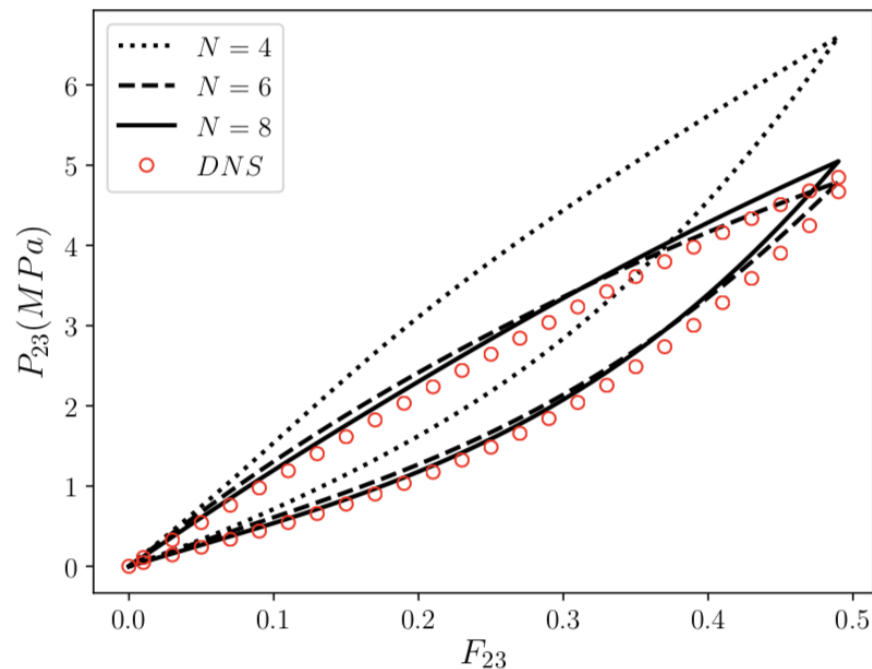(a) $N = 4, N_a = 4, vf_1 = 0.211$ (b) $N = 6, N_a = 13, vf_1 = 0.220$ (c) $N = 8, N_a = 28, vf_1 = 0.224$

- Matrix: Mooney-Rivlin hyperelastic rubber with Mullins effect.
- Particle: Neo-Hookean material which is **100 times harder** than the matrix.
- Large deformation: uniaxial tension up to 50%.


(a) Uniaxial tension.

(b) Shear.

Figure 10: Stress-strain curves from DMN and DNS for hyperelastic particle-reinforced rubber composite with Mullins effect under (a) uniaxial tension and (b) shear loading conditions. Both loading and unloading are considered. The network depth are $N = 4$ (dotted), 6 (dashed) and 8 (solid).

LSTC
Livermore Software
Technology Corp.

Table 7: Offline computational times for the particle-reinforced RVE.

	Training data generation	DMN training (20000 epochs)		
	DNS (400 samples)	$N = 4$	$N = 6$	$N = 8$
N_{cpu}	10	10	10	10
Wall time (h)	39.5	5.4	16.7	43.0
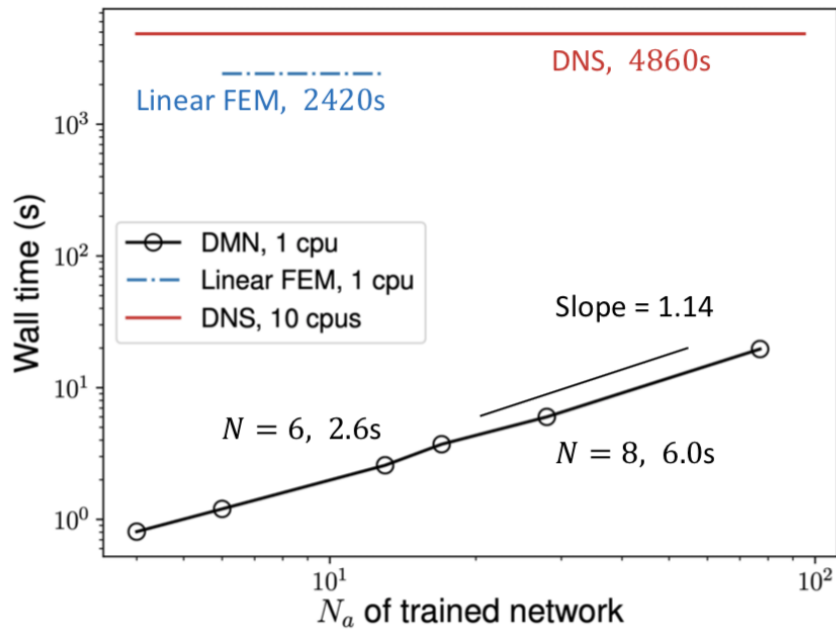
(a) Hyperelastic particle-reinforced composite.

"Computational cost" = $O(N_{dof})$

* Numerical tests are performed on Intel Xeon E5-2640 processor

Schematic of rolling process on a plate

https://materials.imdea.org
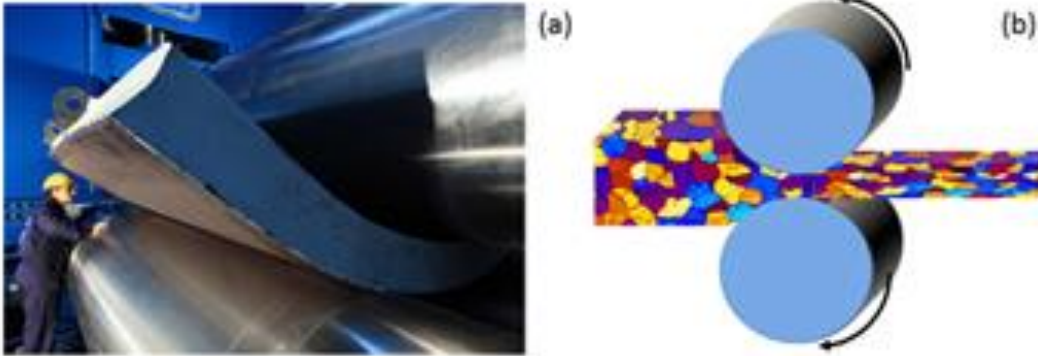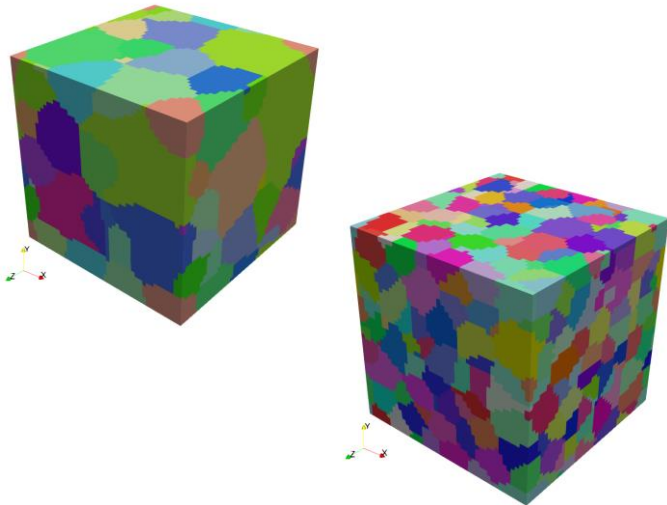
- Macroscale empirical law is not sufficient to describe the anisotropic material behavior under large deformation
- Direct numerical simulation (DNS) of the whole polycrystal structure is prohibited due to large computation cost.

Solution: Reduced order modeling of polycrystal RVE using deep material network
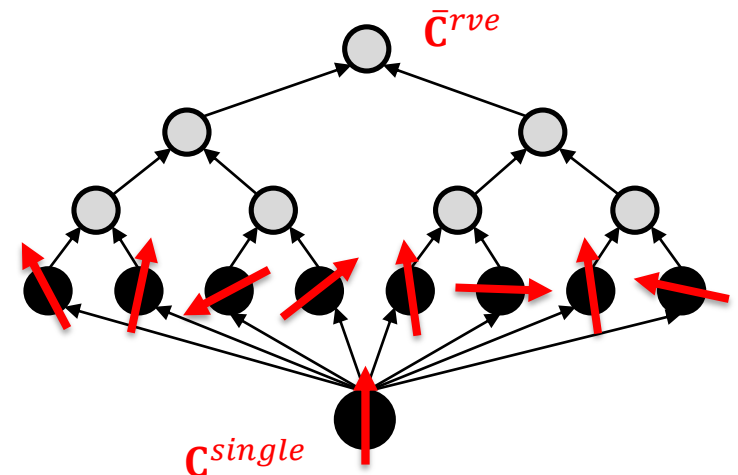

Model reduction / Machine Learning

Deep material network (N=4)
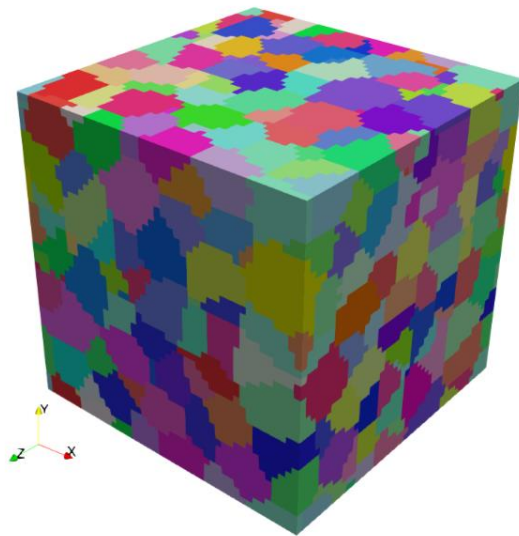
$\bar{\mathbf{C}}^{rve}$

$\mathbf{C}^{single}$

e.g. 45x45x45 FEM mesh

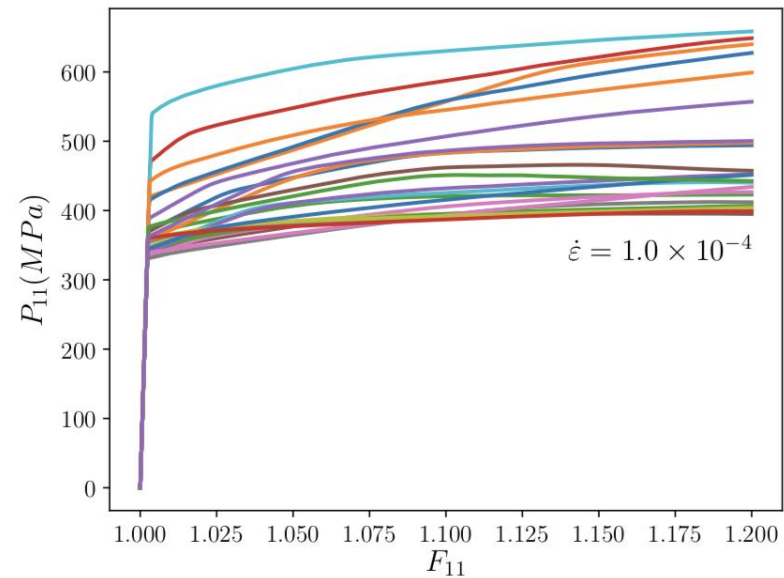**DNS model:** 415 grains, 45 × 45 × 45 mesh, 91125 elements


(a) Geometry and mesh.

(b) Uniaxial-tension responses of single grains (online).

Figure 11: Geometry and single-crystal responses of the polycrystalline RVE with random ODF. In (a), the RVE of equiaxed grains is generated with nominal number 415 and mesh size 45 × 45 × 45. In (b), we selected 25 single grains randomly from the RVE, and pulled them under the crystal plasticity law used in the online stage at strain rate $\dot{\varepsilon} = 1.0 \times 10^{-4}$.

Table 3: Training results of the polycrystalline RVE with random ODF. Average training error $\bar{e}^{tr}$, average test error $\bar{e}^{tr}$ and maximum test error are provided for each DMN.
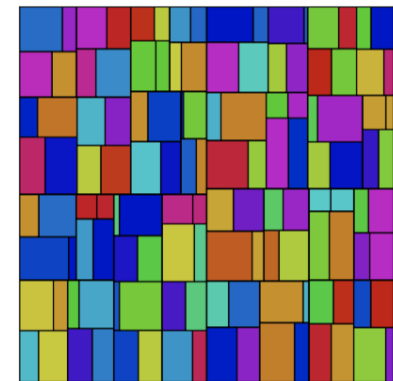
	Epochs	Training $\bar{e}^{tr}$	Test $\bar{e}^{te}$	Maximum e_s^{te}
$N = 4$	20000	5.87%	6.00%	15.5%
$N = 6$	20000	1.16%	1.27%	3.64%
$N = 8$	20000	0.36%	0.43%	1.80%
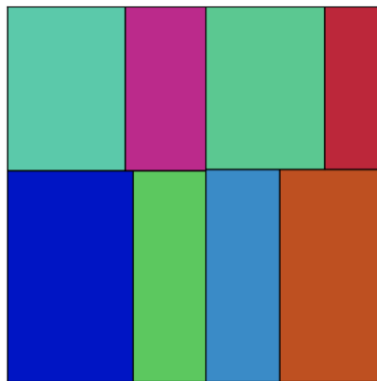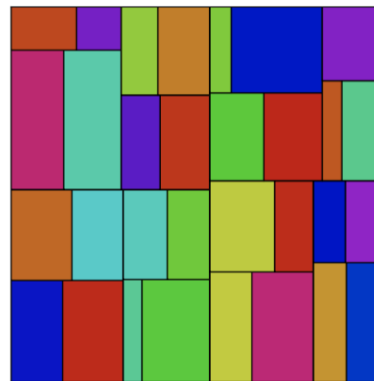
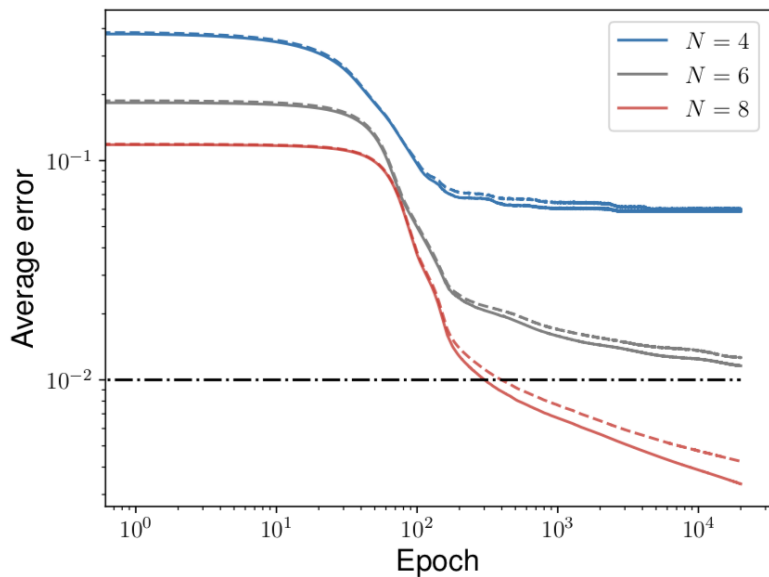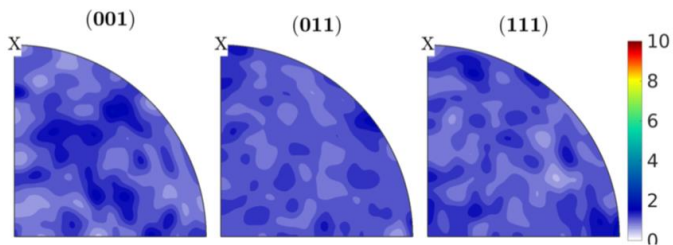(a) $N = 4, N_a = 8$ (b) $N = 6, N_a = 31$ (c) $N = 8, N_a = 128$

Figure 13: Treemaps of DMN for the polycrystalline RVE with random ODF. The network depths N are (a) 4, (b) 6 and (c) 8. The number of active nodes in the bottom layer N_a is listed under each plot. The block colors are randomly assigned.
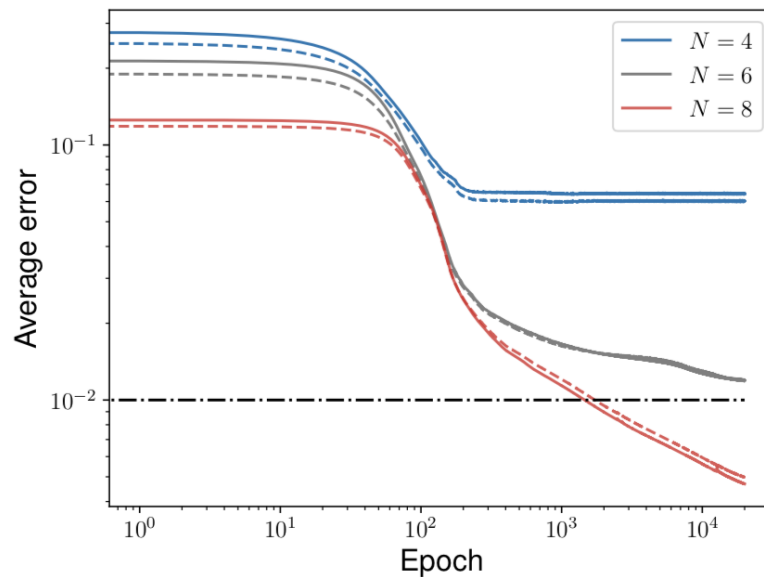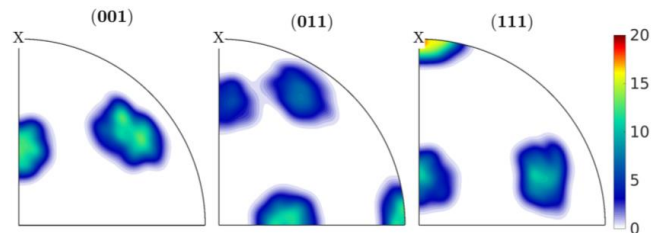
LSTC
Livermore Software
Technology Corp.

RVE with Random ODF

RVE with textured ODF

(a) Random ODF.
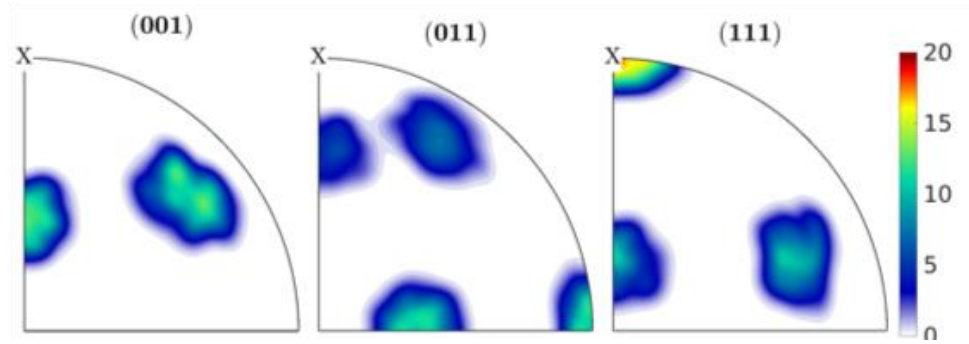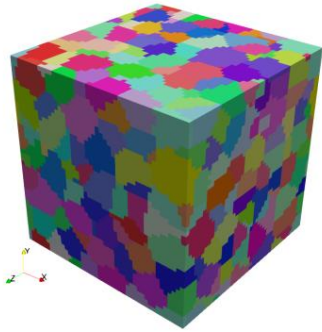
(b) Textured ODF.

Figure 12: Training histories of DMN for polycrystalline RVEs with (a) random ODF and (b) textured ODF. The histories of the average training and test errors are denoted by solid and dashed lines, respectively. All the networks are trained for 20000 epochs.
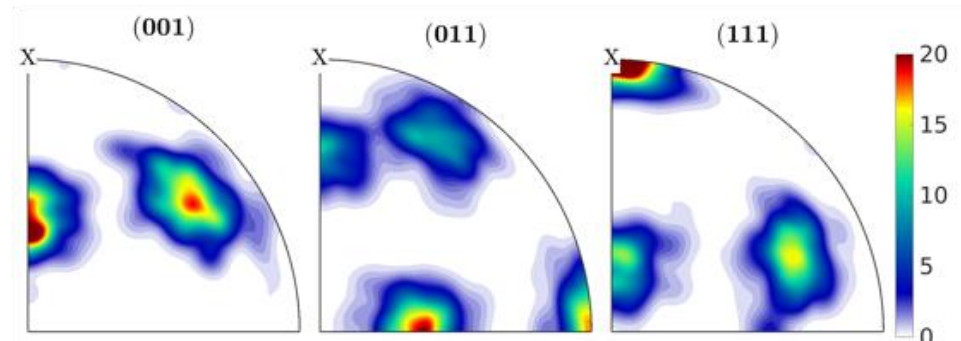
LSTC
Livermore Software
Technology Corp.

Pole figures of DNS *(hidden in data)*

DMN with N = 8

In training ...
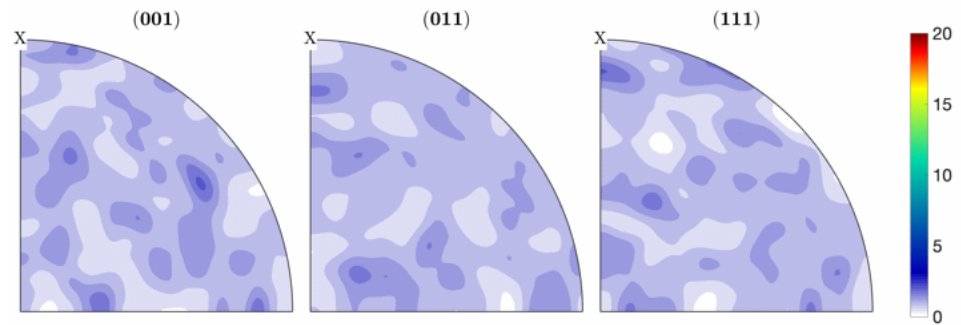
After 20000 epochs,

Deformation gradient

$$\mathbf{F} = \frac{d\boldsymbol{x}}{d\boldsymbol{X}}$$

Decomposition of deformation:

$$\mathbf{F} = \mathbf{F}^e\mathbf{F}^p$$

Evolution of plastic deformation:

$$\dot{\mathbf{F}}^p = \mathbf{L}^p \cdot \mathbf{F}^p$$

Plastic velocity gradient

$$\mathbf{L}^p = \sum_{\alpha=1}^{N_{slip}} \dot{\gamma}_\alpha(\mathbf{s}_\alpha \otimes \mathbf{m}_\alpha)$$

$\dot{\gamma}_\alpha$: shear rate on slip system α
$\mathbf{m}_\alpha$: slip plane normal
$\mathbf{s}_\alpha$: slip direction

Many constitutive laws has been proposed. The following is a phenomenon based one.

Flow rule (power law [1]):

$$\dot{\gamma}^{(\alpha)} = \dot{\gamma}_0 \left| \frac{\tau^{(\alpha)} - a^{(\alpha)}}{\tau_0^{(\alpha)}} \right|^{(m-1)} \left(\frac{\tau^{(\alpha)} - a^{(\alpha)}}{\tau_0^{(\alpha)}} \right)$$

Hardening rule (hardening/recovery law [1]):

Drag stress:

$$\dot{\tau_0}^{(\alpha)} = H \sum_{\beta}^{N_{slip}} q^{\alpha\beta}|\dot{\gamma}^{(\beta)}| - R\tau_0^{(\alpha)} \sum_{\beta}^{N_{slip}} |\dot{\gamma}^{(\beta)}|,$$
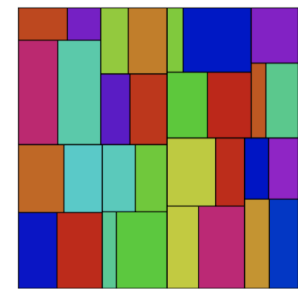
$$q^{\alpha\beta} = \chi + (1-\chi)\delta_{\alpha\beta},$$

Back stress:

$$\dot{a}^{(\alpha)} = h\dot{\gamma}^{(\alpha)} - ra|\dot{\gamma}^{(\alpha)}|,$$
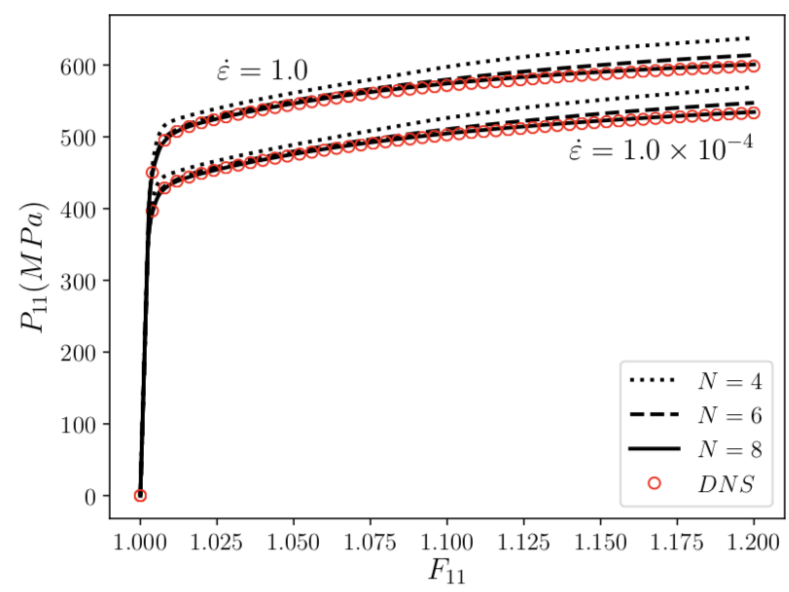
χ, *H*, *R*, *h* and *r* are material parameters.

[1] McGinty, R. D. (2002). Multiscale representation of polycrystalline inelasticity. PhD thesis, Georgia Tech.
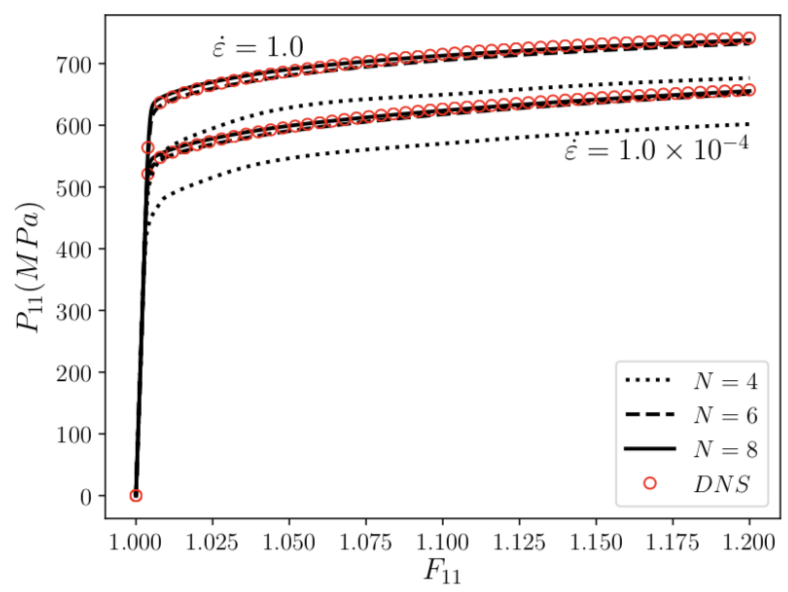
FFT-based DNS: **13 hours (46800s).**

FEM-based DNS: **130 hours (468000s).**

Material network with N = 6: **140s.**

Material network with N = 8: **560s.**

(b) $N = 6, N_a = 31$

(a) Random ODF.

(b) Textured ODF.

Figure 16: Uniaxial stress-strain curves predicted by DNS and DMN for the polycrystalline RVEs with (a) random ODF and (b) textured ODF based on finite-strain rate-dependent crystal plasticity. Two strain rates are considered: $\dot{\varepsilon} = 1.0 \times 10^{-4}$ and $\dot{\varepsilon} = 1.0$. The network depths are $N = 4$ (dotted), 6 (dashed) and 8 (solid).

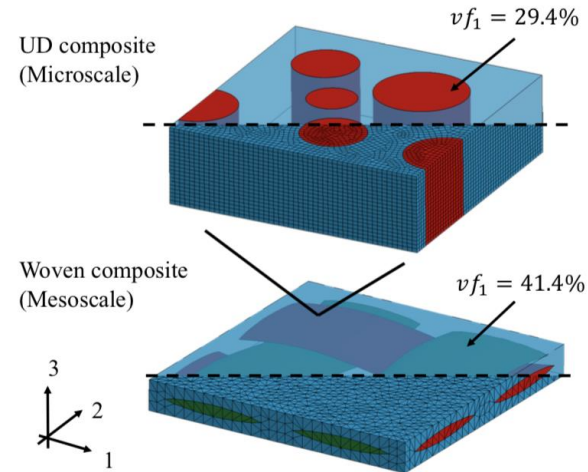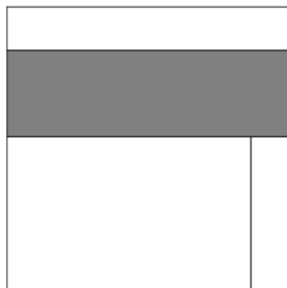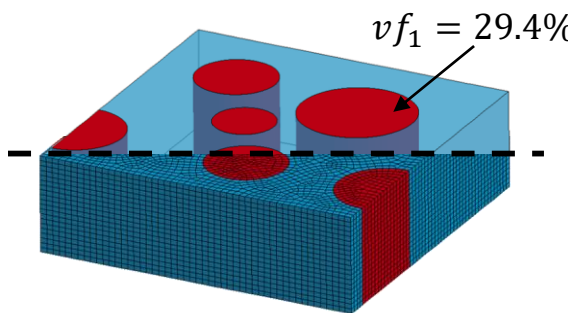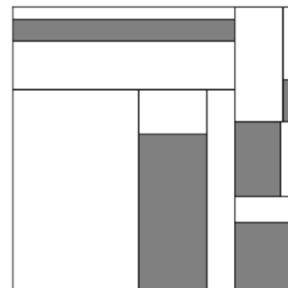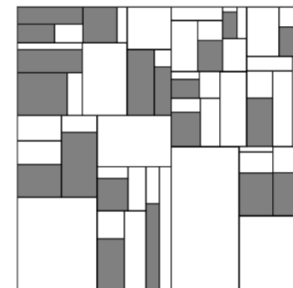Carbon fiber reinforced polymer (CFRP)
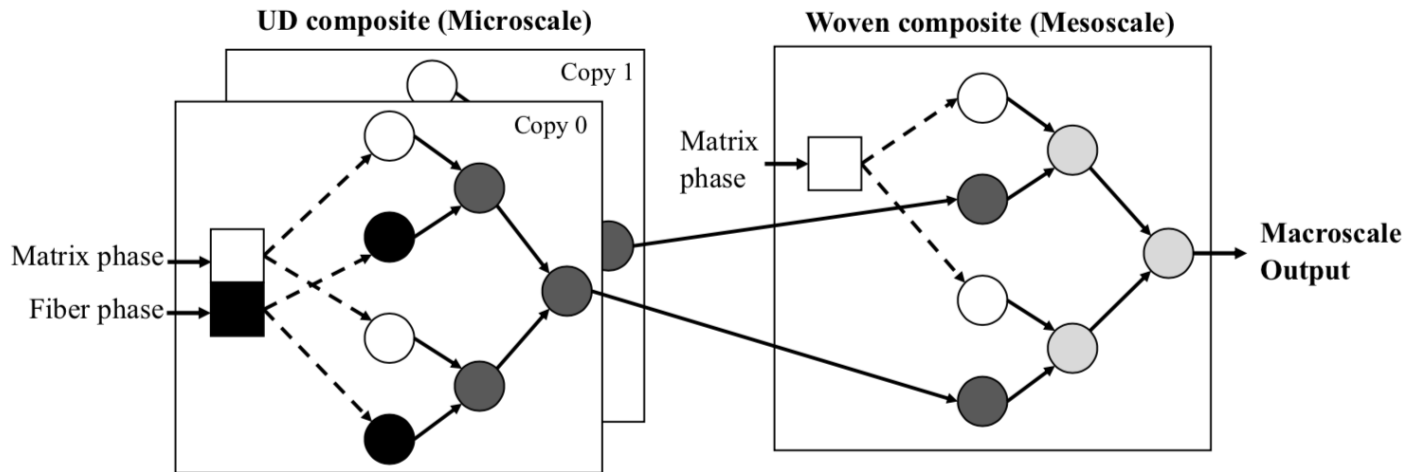
Figure 23: An illustration of three-scale homogenization in CFRP through the concatenation of networks. The material responses of the yarn phase in the mesoscale woven composite are given by the homogenization of the microscale UD composite.
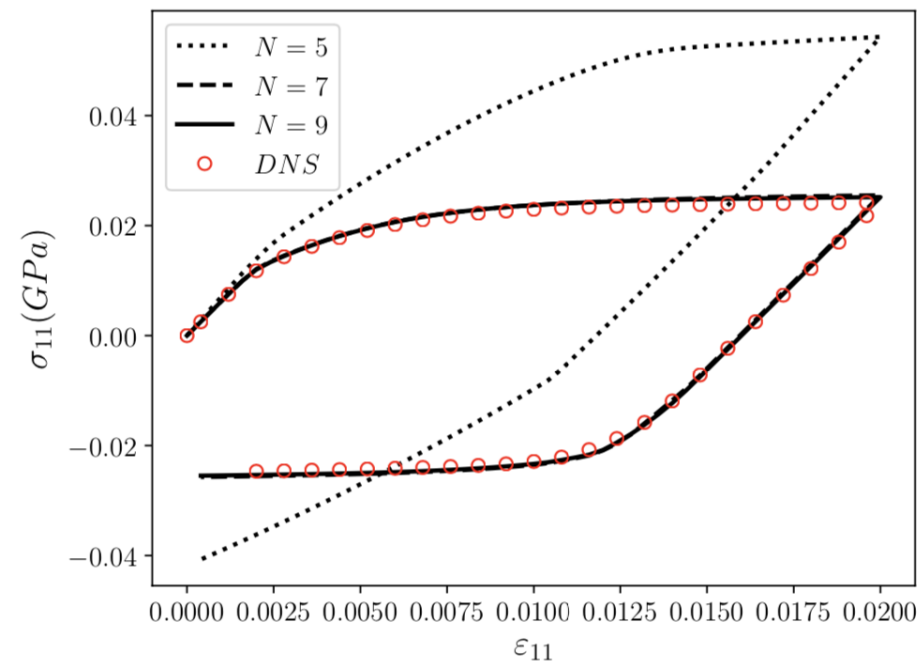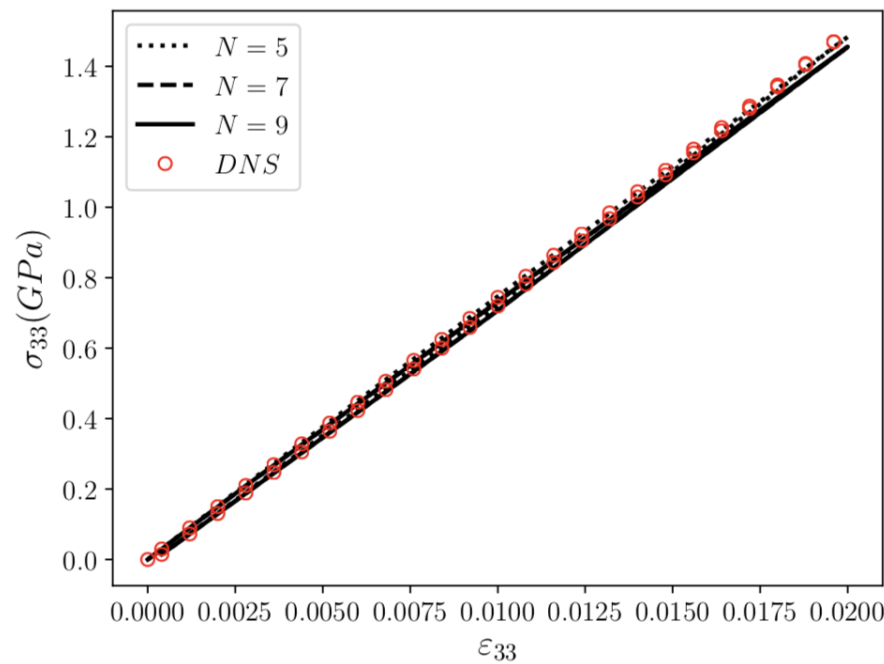
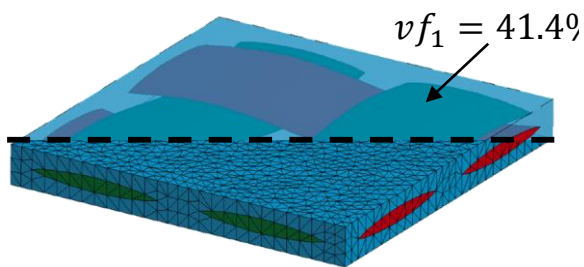(a) $N = 5, N_a = 4, vf_1 = 0.303$ (b) $N = 7, N_a = 14, vf_1 = 0.294$ (c) $N = 9, N_a = 60, vf_1 = 0.295$

(a) σ_{11} vs. ε_{11}

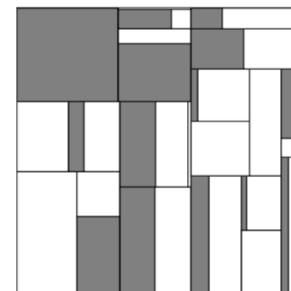(b) σ_{33} vs. ε_{33}
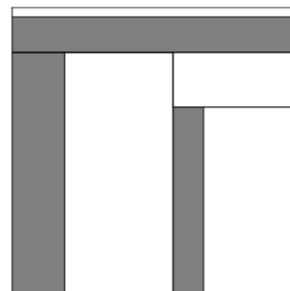
(d) $N = 4, N_a = 3, vf_1 = 0.301$ (e) $N = 6, N_a = 7, vf_1 = 0.348$ (f) $N = 8, N_a = 38, vf_1 = 0.420$

$vf_1 = 41.4\%$

(a) σ_{11} vs. ε_{11}
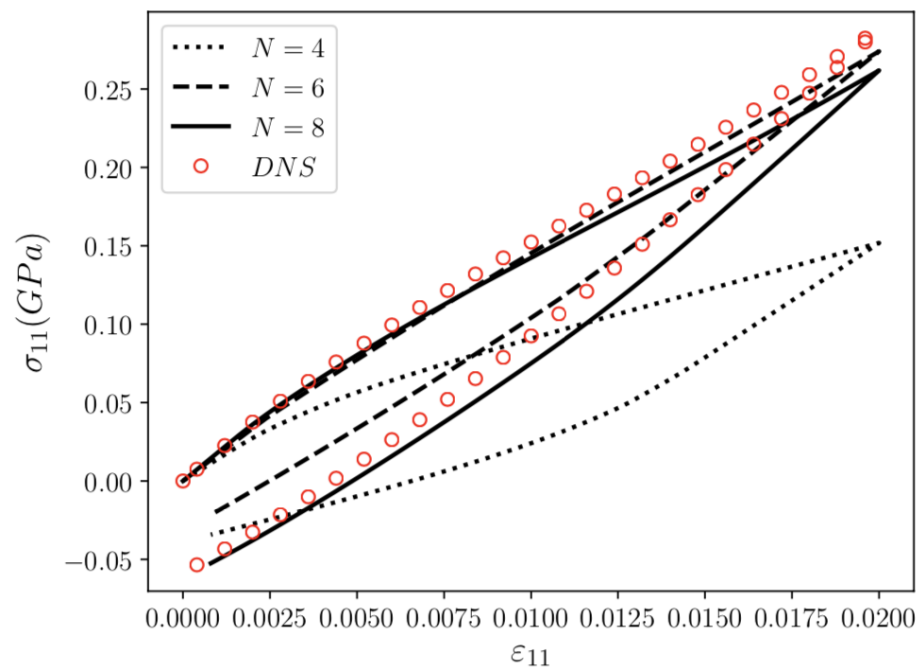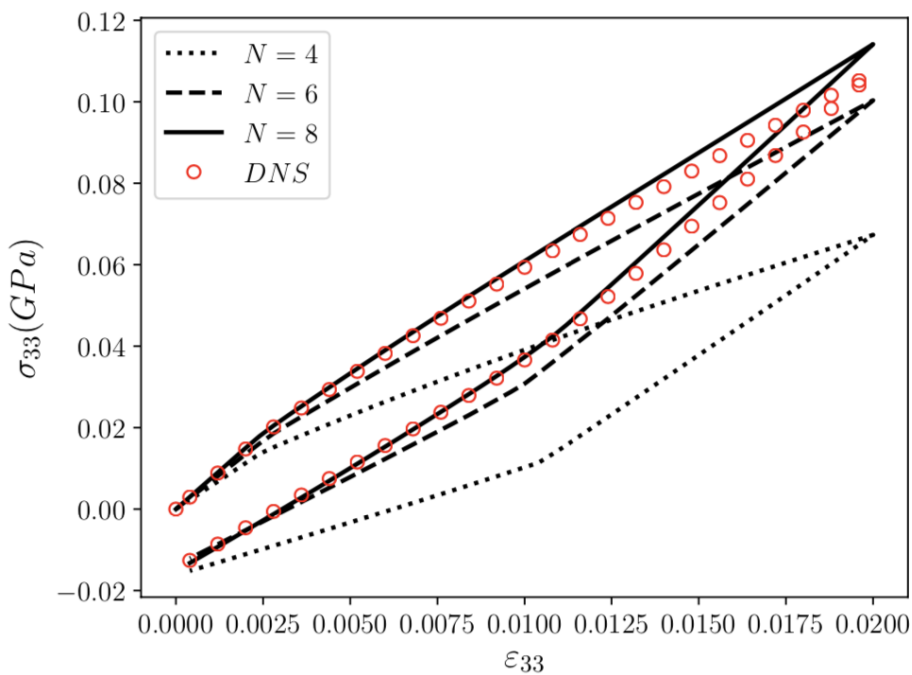
(b) σ_{33} vs. ε_{33}
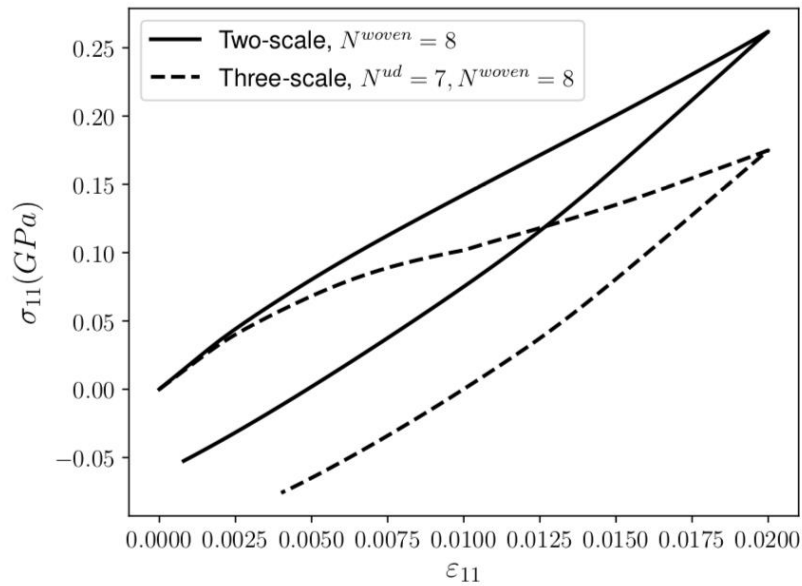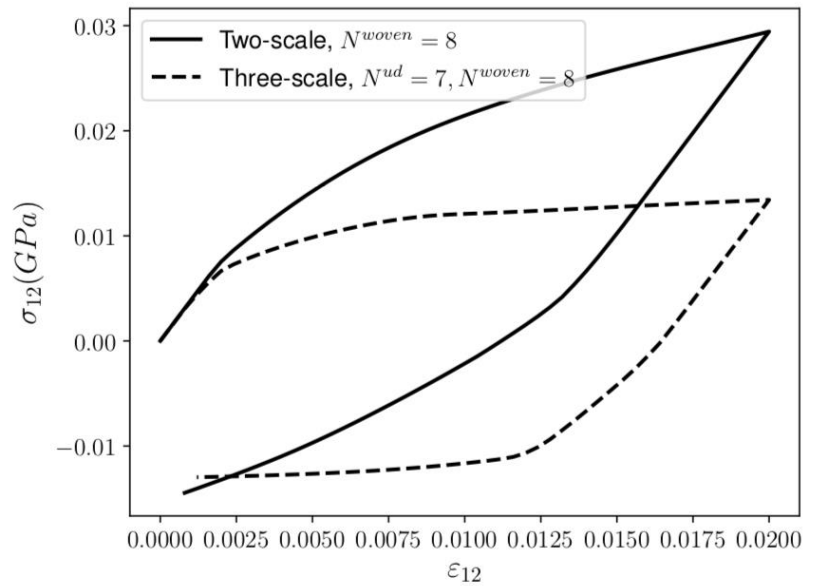
Two Scales: The yarn phase in woven composite is elastic

Three Scales: The yarn phase in woven composite is informed by DMN of UD composite

(a) In-plane tension.
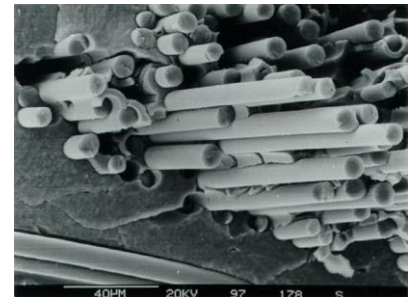
(b) In-plane shear.

Figure 24: Three-scale vs. two-scale homogenizations. The network depths of the UD and woven DMNs are 7 and 8, respectively.

- **Deep material networks**:
  - 2D and 3D building blocks
  - Hierarchical topological structure.
- A complete **machine learning procedure** based on offline numerical DNS data or experimental testing data.
- **Efficient and accurate extrapolation** for challenging RVE homogenization problems:
  - Nonlinear history-dependent plasticity
  - Finite-strain hyperelasticity under large deformations.
  - Crystal plasticity
- **Parallel computing (CPU)**

Future opportunities

- Building blocks with multiple layers / multiple phases
- Interfacial effect : debonding in CFRP, grain boundary effect …
- Integration with design framework
- Concurrent multiscale simulations enhanced by AI/deep material network.
- GPU computing

Thank you!